2020

An Investigation Of Ion Bombardment From Microwave Plasma Chemical Vapor Deposition During Bias Enhanced Nucleation Of Boron-Rich Materials

Bhavesh Ramkorun
University of Alabama at Birmingham

AN INVESTIGATION OF ION BOMBARDMENT FROM MICROWAVE PLASMA CHEMICAL VAPOR DEPOSITION DURING BIAS ENHANCED NUCLEATION OF BORON-RICH MATERIALS

by

Bhavesh Ramkorun

Dr. Shane A. Catledge, CHAIR
Dr. Manoj K. Mahapatra
Dr. Mary E. Zvanut

A THESIS

Submitted to the graduate faculty of The University of Alabama at Birmingham,
in partial fulfillment of the requirements for the degree of
Master of Science

BIRMINGHAM, ALABAMA

2020

AN INVESTIGATION OF ION BOMBARDMENT FROM MICROWAVE PLASMA CHEMICAL VAPOR DEPOSITION DURING BIAS ENHANCED NUCLEATION OF BORON-RICH MATERIALS

Bhavesh Ramkorun

PHYSICS

ABSTRACT

This study involves an Ar/H_2 plasma acting on a negatively DC-biased silicon substrate in a microwave plasma chemical vapor deposition. The flow rate of hydrogen was constant at 500 sccm, and that of argon was varied between 0 sccm and 500 sccm. Bias current was recorded for several values of the applied bias voltage ranging from – 100V to – 340V. At 10 and 20 torr, a peak in the bias current was found as argon flow rate changed. A decrease in current with varied argon intensity in glow discharge plasma has been reported in the literature. Our results substantiate these results, and further show a peak in bias current. OES data was used to estimate the plasma electron temperature which was found to be constant at each pressure. This suggests that the observed peak in bias current may be due to variation in plasma density as Ar flow changes between 0 sccm and 500 sccm. Using these results, substrate bias pre-treatment experiments were performed at 10 torr in an Ar/H_2 plasma, yielding the maximum bias current. Nucleation density of boron deposits were measured after subsequent exposure to B_2H_6 in H_2 plasma and found to be a factor of 200 times higher than when no bias and no argon was used. Experiments were repeated at 20 and 30 torr (fixed bias voltage and Ar flow rate) in order to test the effect of chamber pressure on the nucleation density. Compared to 30 torr, we find nearly 7 times higher boron nucleation densities for both 10 and 20 torr pressures

when using DC bias in the Ar/H2 plasma. Results are explained by incorporating measurements of plasma optical emission and by use of heterogeneous nucleation theory. Overall, these results help identify optimal conditions for nucleating and potentially growing superhard boron-rich coatings.

Keywords: Microwave plasma chemical vapor deposition, Heterogenous Nucleation, Bias enhanced nucleation, Nucleation density, Boron-rich materials, Electron Temperature

DEDICATION

I dedicate this work to God who worked in me during the past 2 years in Birmingham, my church 'Covenant Presbyterian Church', and my parents, especially my father who is still alive today due to God's sovereign goodness.

ACKNOWLEDGMENTS

I thank Dr. Catledge for being a great mentor. He is knowledgeable and creative in his field. He is also friendly and compassionate. He has realistic goals and expectations. He had the idea of implementing a DC bias in the 6kW microwave plasma chemical vapor deposition which he conveyed to me in summer 2018. Since then, he gave me a lot of freedom to explore the science involved, to present them at four conferences, and to write them academically in a paper. Thank you for allowing me to join your lab to work on this master's thesis.

I thank Kallol Chakrabarty, PhD student in Dr. Catledge's lab, for always having an open door. It was a pleasure working alongside you for the past 2 years, drinking tea with you every day, and going to lunch buffet regularly.

I thank Dr. Mary E. Zvanut, physics graduate program director, for actively listening and understanding about my career goals, and for supporting me to seek them. You doing so has allowed me to do well in my research work at UAB.

I thank Dr. Paul Baker for every intellectual conversation about CVD, XPS, XRD, plasma diagnostics, crystallites, nucleation and so much more. You have challenged me a lot to re-consider my scientific thoughts and ideas.

This material is based upon work supported by the National Science Foundation (NSF) EPSCoR RII-Track-1 Cooperative Agreement OIA-1655280. Any opinions, findings, and conclusions or recommendations expressed in this material

are those of the authors and do not necessarily reflect the views of the National Science Foundation.

TABLE OF CONTENTS

Page

LIST OF TABLES

LIST OF FIGURES

Figures *Page*

LIST OF ABBREVIATIONS

(Entries are listed alphabetically)

Ar	Argon
Ar_{706}	Argon emission line at 706 nm
Ar_{750}	Argon emission line at 750 nm
Ar/H_2	Argon/Hydrogen
B_2H_6	Diborane
BEN	Bias enhanced nucleation
CVD	Chemical vapor deposition
DC	Direct current
eV	Electronvolt
H_2	Hydrogen
H_α	Hydrogen alpha
H_β	Hydrogen beta
H_γ	Hydrogen gamma
IR	Infrared red
kW	kilowatt
MPCVD	Microwave plasma chemical vapor deposition
OES	Optical emission spectroscopy
sccm	Standard cubic centimeters per minute
T_s	Substrate temperature
T_e	Electron temperature
XPS	X-ray photoelectron spectroscopy

CHAPTER 1: INTRODUCTION

1.1 Hypothesis

Heavy ion bombardment, for example from argon, can sputter a silicon substrate and create nucleation sites on it. Further ion bombardment from reactive species such as boron will allow heterogenous nucleation on the substrate. Bias enhanced nucleation (BEN) has been used to nucleate and grow carbon containing materials, and similar technique can be used to nucleate of boron-rich materials. This will be investigated using ion bombardment in chemical vapor deposition (CVD).

1.1.1 Testing the hypothesis

Argon's heavy mass makes it favourable for use in sputtering as it transfers more energy to a target through change of momentum [1]. A silicon substrate that has been sputtered has nucleation sites onto which heterogamous nucleation takes place. These substrates will be exposed to B_2H_6 for 15 minutes to allow nucleation of boron-rich materials. Substrates bombarded with argon ions prior to nucleation will be compared to control substrates that are not bombarded prior to nucleation. Substrates will also be negatively biased using DC bias to allow for BEN. Substrate that have been biased will be compared to substrates that have not. The nucleation will be imaged under optical microscopy and the nucleation density will be analyzed by counting the number of

nucleation per unit area. The nucleated materials will be analyzed using X-ray photoelectron spectroscopy (XPS) to determine percentage of boron present.

1.2 Motivation

Diamond is currently the hardest material that exists in nature, and therefore is popular in industry operations including, but not limited to, cutting, drilling, and grinding. However, diamond is oxidized at 600°C, and is converted into graphite at 900°C [2]. Therefore, the industry use of diamond is restricted.

There is a high interest to study boron-rich materials. This is because many polymorphs of boron have a high hardness. Crystal structures of at least 4 pure boron phases have been reported in literature: $\beta - B_{106}$, $\alpha - B_{12}$, $T - 192$, and $\gamma - B_{28}$ of hardness of at least 45 GPa, 42 GPa, 30 GPa, and 50 GPa respectively [3]. These contain B_{12} isocahedra (12 atom clusters).

The basic structure of these compounds is also icosahedra. These compounds are analogous to carbon polymorphs and are therefore diamond-like and/or graphite-like. Cubic boron nitride and wurtzitic boron nitride demonstrated sp^3 covalent bonding similar to diamond. They both exhibit high hardness of at least 40 GPa [4]. Boron suboxides have demonstrated high hardness between 32 and 60 GPa.

Given the super hardness of boron, and boron-rich materials, these materials have a wide range of application in high pressure and high temperature environment. Icosahedral boron-rich materials have a melting temperature of up to 2400°C. The

electric conductivity of boron carbide is measured between 77 and 1200 K [5]. These carbides can have anywhere between 9% and 20% carbon. The focus of research on creating boron-rich materials research work is primarily important because these materials can replace diamond in industry applications.

Boron rich materials have mainly been created and studied by high pressure-high temperature techniques, such as by carbothermic reduction, magnesiothermic reduction [6] and diamond anvil cell [7]. However, it is also possible to create boron-rich materials by low pressure-low temperature techniques, such as CVD. The study of nucleation of boron-rich materials by microwave plasma-CVD (MP-CVD) is lacking in literature and hence the topic of this research.

1.3 Literature Review

In CVD deposition of diamond films on silicon substrates, diamond slurry is often used to scratch the silicon surface in order to enhance nucleation through formation of high surface energy nucleation sites [8]. The growth rate of diamond on polished silicon wafers is usually not as successful as on wafers where deliberate surface damage was made [9]. Such nucleation sites can decrease the work required for nucleation of a cluster of critical radius in heterogenous nucleation.

A DC bias also been used to pre-treat a silicon substrate in order enhance nucleation. This process was first explored in CVD nucleation of diamond in 1991, whereby a silicon substrate was pre-treated for several minutes in a high methane plasma where a negative

bias voltage was applied to the substrate [10]. This process became known as BEN. Applying a negative DC bias to a substrate creates an electric field, thus directing the motion of ions towards the substrate [11]. Usually, the substrate is the cathode and the MPCVD chamber is the anode. This method has led to a higher nucleation density when compared to substrates that have been scratched by diamond [12]. While BEN was first used to nucleate and grow diamond in CVD, it was soon used to nucleate and grow cBN [13]. Here, BEN of boron rich materials will be studied.

1.4 Heterogenous Nucleation

In MP-CVD, phase transformation occurs between vapor and solid for nucleation to occur on a substrate. An energy barrier, W^*, must be overcome for a cluster of critical size to be nucleated. A nucleation of this critical size is favored to complete the phase transformation. The number of clusters passing this critical size per unit time is the nucleation rate, I^{st}, given by [14]:

$$I^{st} = N\,K\,Z \exp\left(\frac{-W^*_{net}}{k_B T_s}\right) \ldots\ldots\ldots\ldots\ldots\ldots [1]$$

N is the number of ions or molecules present. K is the rate at which the ions or molecule bombard a substrate onto which nucleation occurs. Z is the Zeldovich factor, which is inversely proportional to the square root of the substrate temperature, T_s, during nucleation. Z gives the probability that a nucleus will form a new phase (nucleation) than dissolve. k_B is the Boltzmann constant. W^*_{net} can be decreased by using

argon as described above. In order to increase K, maximum ion bombardment needs to occur on the negatively biased substrate.

Studies have shown that in a glow discharge, electrical current between electrodes varies with the concentration of hydrogen added to an argon plasma, such that the current due to ions decreases non-linearly with increased concentration of hydrogen [15]. The current also varies such that there is a higher current flow at 10% hydrogen in the Ar/H_2 plasma than there is at 1% hydrogen, and that there is even higher current at 0% hydrogen. In order to maximize K in the Ar/H_2 plasma in the CVD, an investigation of the current flowing through the silicon substrate with varying argon and hydrogen concentration was studied.

CHAPTER 2: MATERIALS AND METHODS

2.1 Experimental Design

2.1.1 Microwave Plasma Chemical Vapor Deposition

In CVD, chemical vapor from a gas precursor nucleate and grow into materials on the surface of a heated substrate. The temperature of the substrate typically ranges from 200^{o}C to 1600^{o}C. The temperature of the substrate can be recorded using an IR pyrometer. The reaction usually occurs at sub atmospheric pressure, such as 10 – 90 torr.

In MPCVD, a microwave is used to ignite a plasma, from which ions bombard a substrate's surface where nucleation occurs. H_2 is used as the initial gas in the plasma. Then B_2H_6 is introduced, a reactive gas that has been used to grow boron rich materials. The plasma allows materials to be nucleated on substrate of lower temperature through metastable species [16]. Species of the gas, which get dissociated by the plasma, are adsorbed on the surface of the substrate and react to form nuclei. Here, the number of nuclei per unit area, nucleation density, was analyzed for boron rich materials.

The microwave power of the MPCVD was constant at 0.6 kW. The hydrogen flow rate was constant at 500 sccm. The argon flow rate was varied between 0 and 500 sccm. Initially, the experiment was run at 10 torr. A schematic view of the MPCCVD is shown in Fig 1.

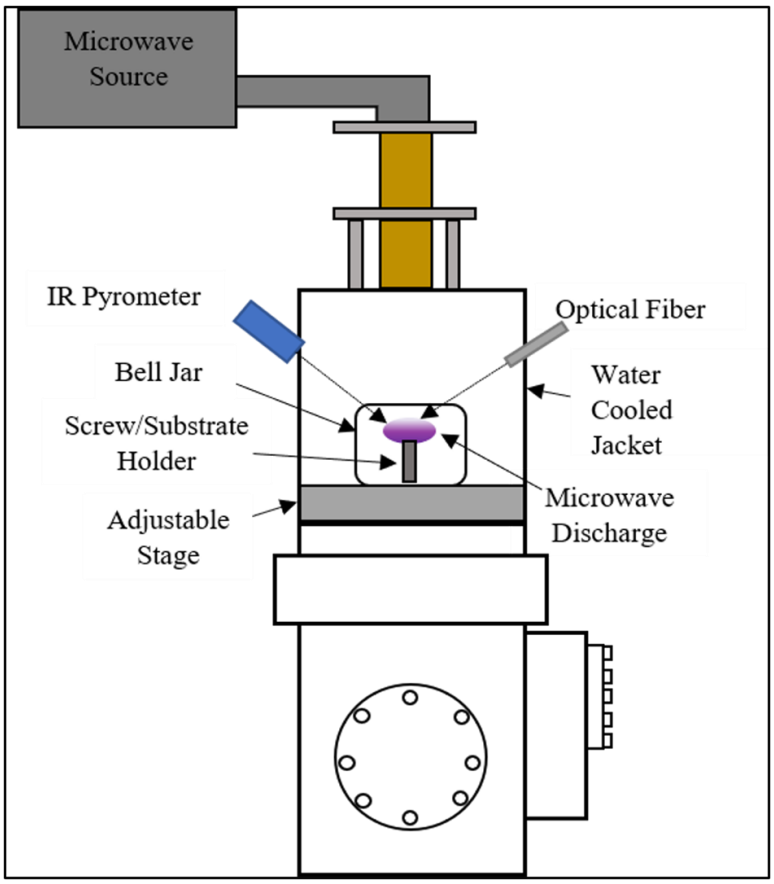

Fig 1: Schematic view of the CVD set up. A microwave source provides the microwave to ignite the plasma above the substrate. An IR pyrometer is used to record substrate temperature. Optical fiber transport light from the plasma to OES analysis.

2.1.2 Bias Enhanced Nucleation

The rate at which ions bombard the substrate can be controlled by using a DC bias, where the substrate is negatively charged and the shell of the MPCVD is grounded. This creates an electric field in the plasma and positively charged ions accelerate towards the substrate due to the field. As mentioned in section 1.4, ions bombarding a silicon

substrate leads to heterogenous nucleation. BEN allows ions to bombard substrate at a higher rate, which can lead to a higher nucleation rate. A schematic view of the MPCVD with the DC bias setup is shown in Fig 2.

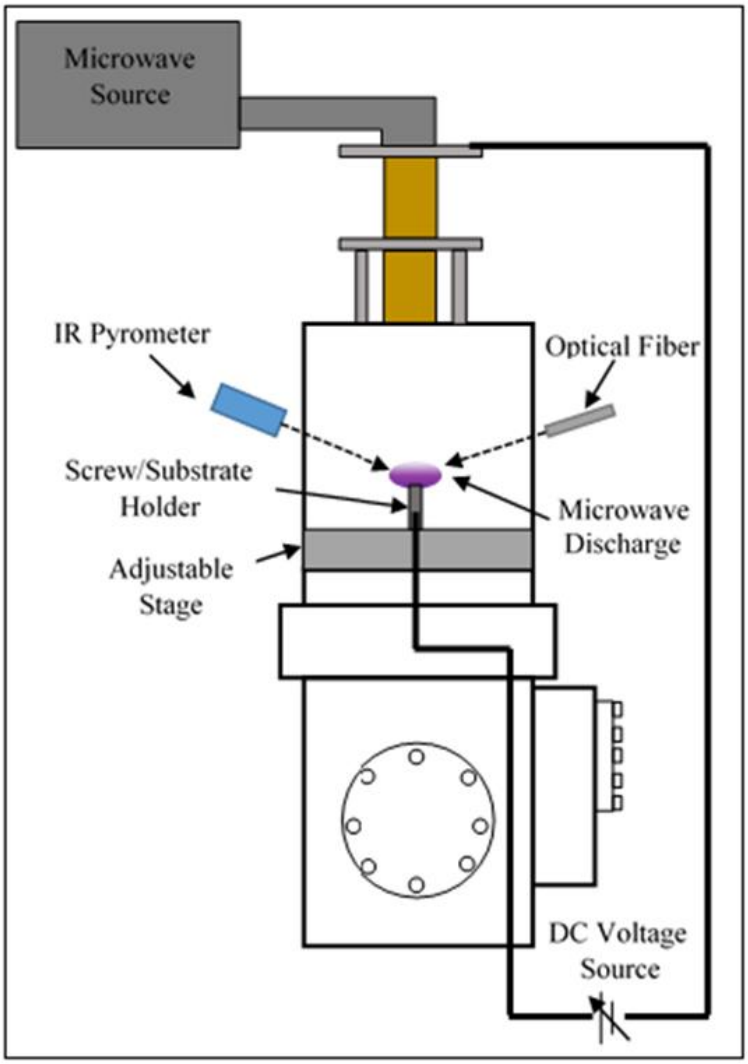

Fig 2. Schematic diagram of DC Bias added to the CVD. The substrate is negatively biased, and the CVD chamber is grounded. This creates an electric field which allow ions

from the plasma to bombard the substrate. The voltage can be controlled and the current going through the substrate can be recorded.

The bias voltage of the silicon substrate was constant at – 250 V. The CVD chamber was grounded. For each increment of argon flow rate, the current flowing through the substrate was recorded to find any peak in current. The measurement of current was then repeated at 20 and 30 torr to find any observable peak in current.

After a maximum current was found at 10 torr for a flow rate of argon, the silicon substrate was pretreated for 30 minutes in the Ar/H_2 plasma. Argon was then turned off and diborane (5% B_2H_6 in H2) was introduced at a flow rate of 2 sccm to the pure hydrogen plasma (500 sccm) for 15 minutes in order to nucleate high boron content material on the pretreated silicon substrate. The silicon substrate was viewed under an optical microscope at 100X magnification. The corresponding image was converted into binary image using ImageJ [17, 18]. Image contrast was adjusted such that the silicon substrate was set to white and the nuclei set to black. The number of nuclei per unit area was counted using the ITCN plug in ImageJ [19]. The above experiments were repeated for chamber pressure of 20 and 30 torr in order to test for the effect of pressure on nucleation density.

2.2 Microwave Plasma

2.2.1 Properties of the Plasma

The energies of electrons and ions in a plasma can be represented in terms of their temperature. In a plasma the electrons and ions can have different velocity distributions which translates into different temperatures in a plasma. Typically, the electron temperatures are on the order of 1- 10 eV, and the ion temperatures are on the order of 0.1 eV.

In MPCVD, the microwave driving frequency, $\nu_{mw} = 2.45$ GHz, is the frequency at which electrons oscillate in the plasma due to electromagnetic field. Since ν_{mw} is fixed, the maximum electron density, ρ_e, can be calculated to be 7.46×10^{16} m^{-3}, according to equation below: [20]

$$\rho_e = \frac{m_e \epsilon_o (2\pi\nu_{mw})^2}{e^2} \text{..... [2]}$$

ϵ_0 is the permittivity of free space, e is the electronic charge, and m_e is the electronic mass. Therefore, the electron average distance, $\lambda_n = \frac{1}{(\rho_e)^{\frac{1}{3}}}$, is approximately 2.4×10^{-6}m and the maximum mutual potential energy of electrons and ions, $\frac{e^2}{4\pi\epsilon_0\lambda_n}$, is $1.00 \times 10^{-22} J$. Assuming a maximum electron temperature ,T_e of 10 eV, the maximum average kinetic energy of the electrons in the plasma, $\frac{3}{2}k_B T_e$, is 1×10^{-18} J, where k_B is the Boltzmann constant. Since the mutual potential energy of electrons and ions is much

smaller than the average kinetic energy of the electron, the plasma is cold and follows ideal gas law [21].

2.2.2 Optical Emission Spectroscopy

The gases flowing in the plasma are often dissociated into a broad spectrum of molecules that are both neutral and ionized. The plasma in CVD is a glow discharge. The term glow discharge arises because atoms excited by electron, release energy in the form of photons when they relax; the photons produce the glow. The plasma is luminous, and optical emission spectroscopy (OES) can be used to characterize the intensity of species in the plasma. OES was recorded in the wavelength range 300 nm to 900 nm. Fig. 3 – 6 shows OES spectra recorded at 10 torr for varying Ar flow rate and DC bias voltage.

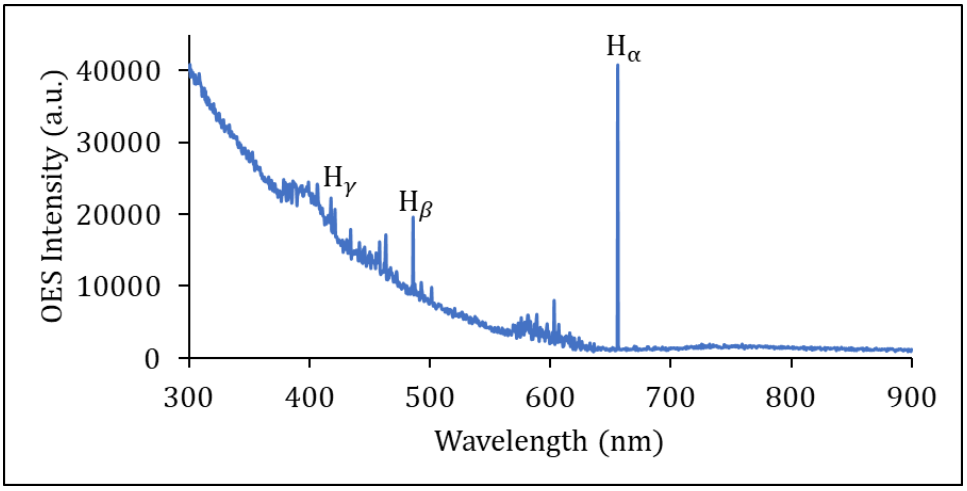

Fig 3: OES spectrum at 10 torr, 0 sccm Ar, -100 V DC Bias.

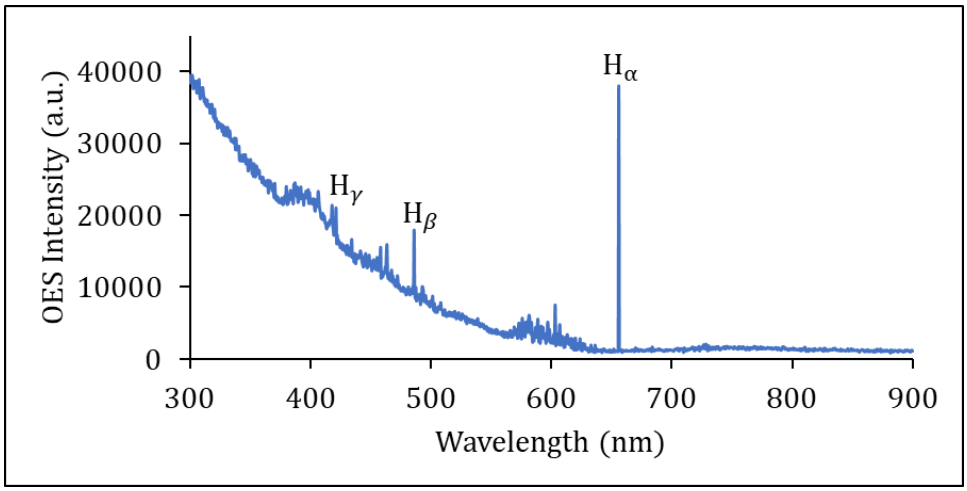

Fig 4: OES spectrum at 10 torr, 0 sccm Ar, -260 V DC Bias.

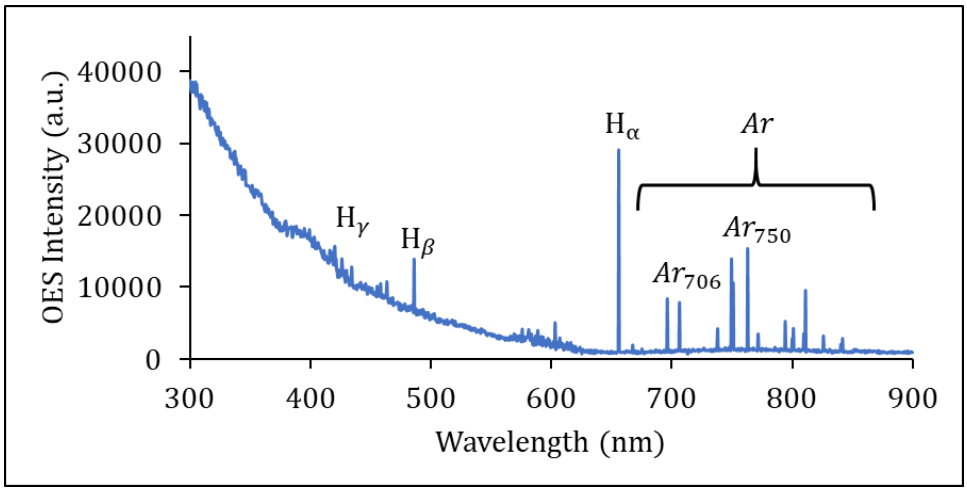

Fig 5: OES spectrum at 10 torr, 500 sccm Ar, -100 V DC Bias.

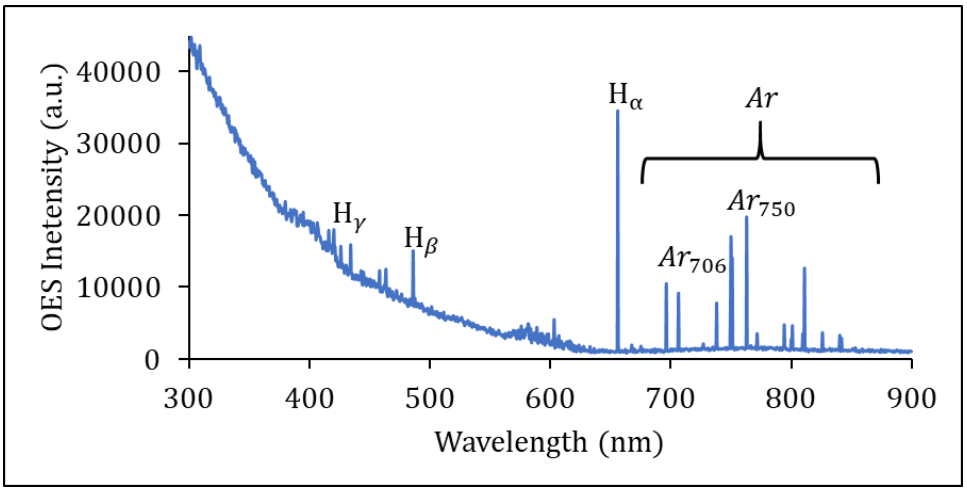

Fig 6: OES spectrum at 10 torr, 500 sccm Ar, -260 V DC Bias.

Since the flow rate of Ar, and the bias voltage is varied, Fig 7 shows the ratio of H_α/H_γ for different argon flow rate and different bias voltages. The ratio has been calculated 5 times, and the standard deviation is used as error bars. The data suggest that the ratio of H_α/H_γ remains constant regardless of Ar flow and bias voltage.

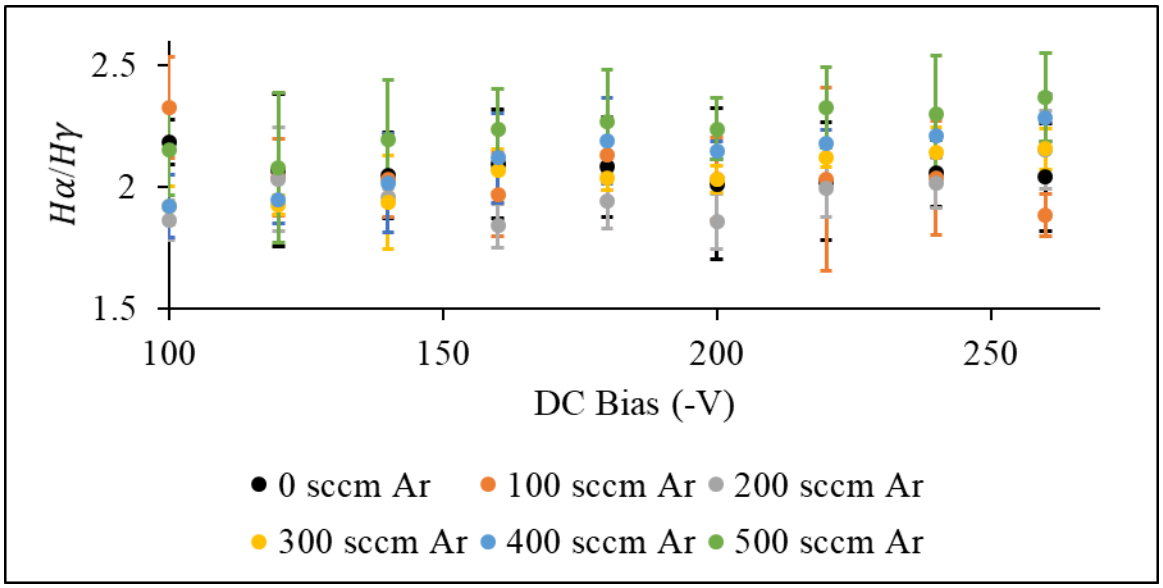

FIG 7: H_α/H_γ with varying DC bias for several Argon flow rate at 10 torr.

Similarly, Fig 8 shows the ratio of Ar_{750}/Ar_{706} for varying Ar flow rate and bias voltage. Ar_{750} is the highest peak of Ar in the OES, comparable to H_α and Ar_{706} is the lowest peak of Ar in the OES, comparable to H_γ. The results indicate the ratio of Ar_{750}/Ar_{706} does not change regardless of Ar flow and bias voltage.

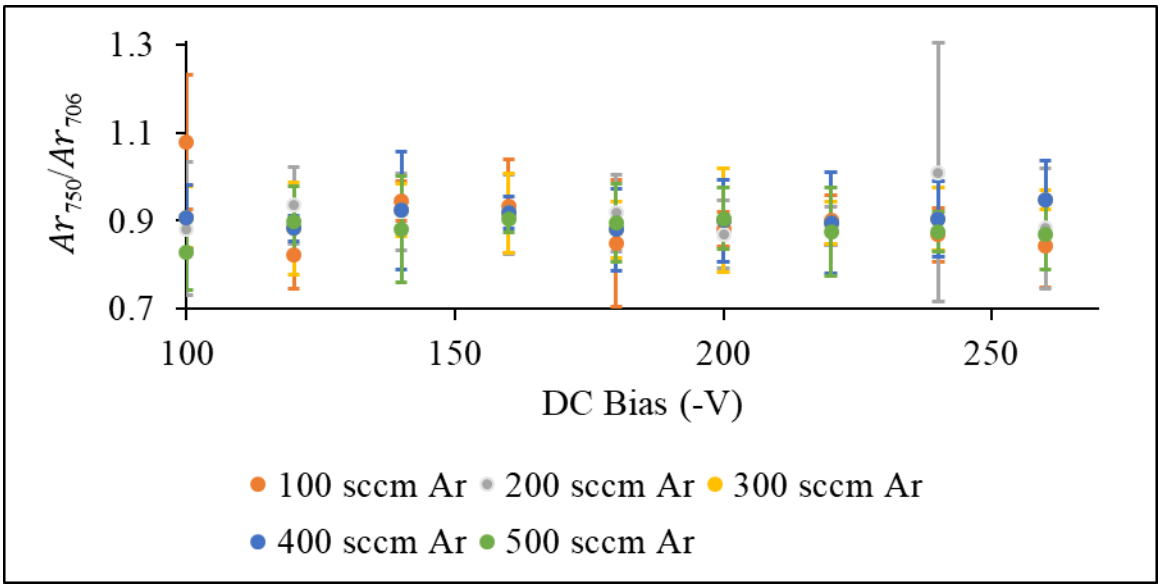

FIG 8: Ar_{750}/Ar_{706} with varying DC bias for several Argon flow rate at 10 torr.

Similarly, OES spectra were taken at 20 and 30 torr. The results indicate that the ratio of H_α/H_γ and Ar_{750}/Ar_{706} does not change at those pressure. These results show that not one individual OES line of H_2 or Ar is affected differently from increase Ar flow.

Ar_{750}, was compared to H_α. The ratio increases linearly with increased flow rate of argon at each pressure, shown in Fig. 9. This results indicate the intensity of Ar in the plasma increases linearly with increased Ar flow at each pressure.

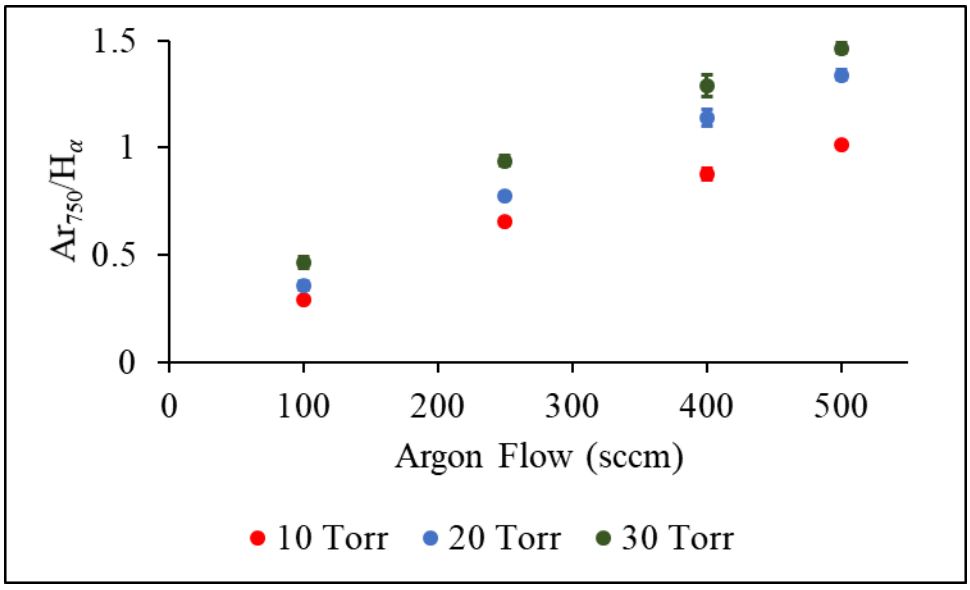

Fig 9: Linear increase of the ratio of argon to hydrogen alpha at 10, 20 and 30 torr.

CHAPTER 3: RESULTS AND DISCUSSION

3.1 Results

3.1.1 Current

First, the current was recorded for varying flow rate of Argon at different voltages. Fig 10 shows such graph at 10 torr. The corresponding variation of current against bias voltage is shown in Fig 11. Similarly, Fig 12. and Fig 13 shows data for 20 torr, and Fig 14. and Fig 15. Shows data for 30 torr.

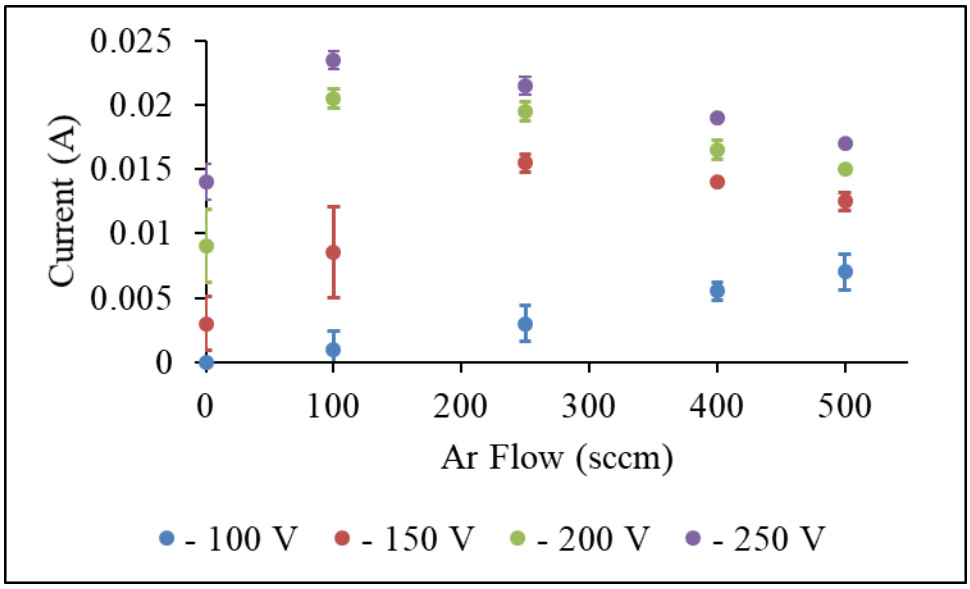

Fig 10: Current against flow rate for varying argon flow at 10 torr.

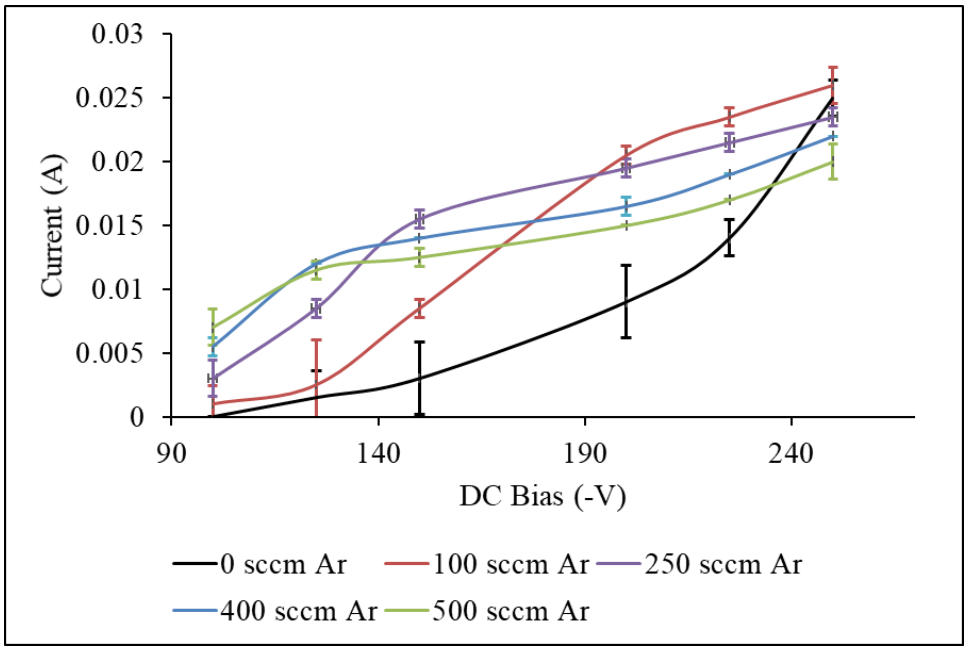

Fig 11: Current against bias voltage for different argon flow at 10 torr.

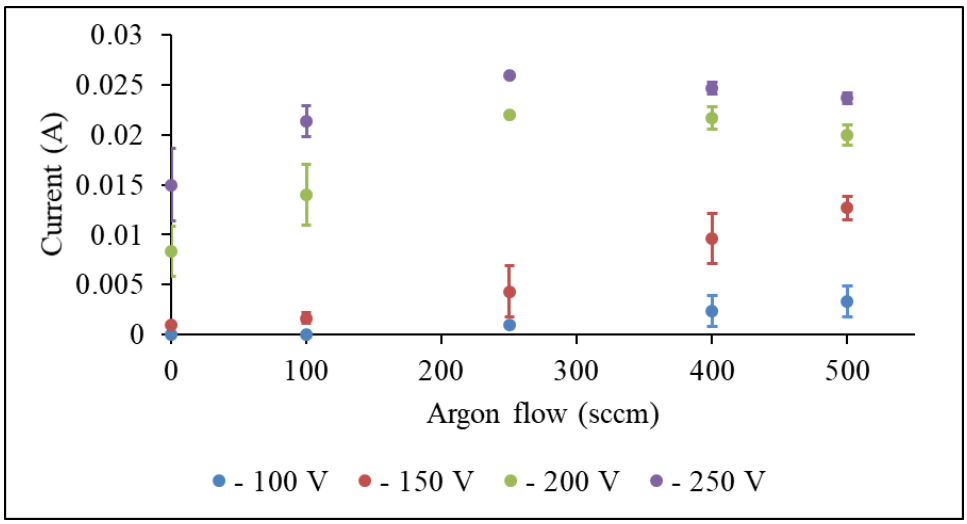

Fig 12: Current against flow rate for varying argon flow at 20 torr.

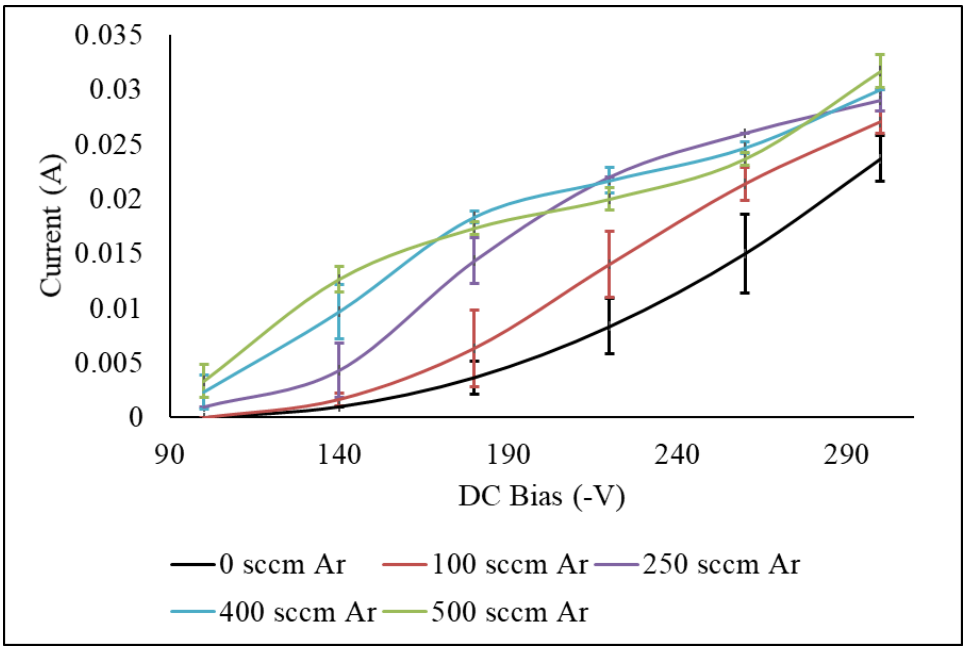

Fig 13: Current against bias voltage for different Ar flow at 20 torr.

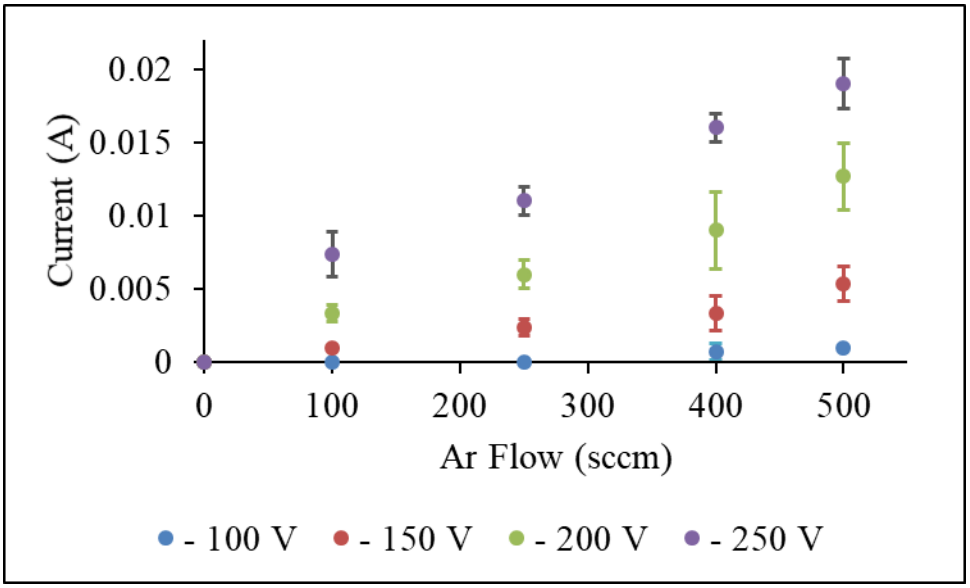

Fig 14: Current against flow rate for varying argon flow at 30 torr.

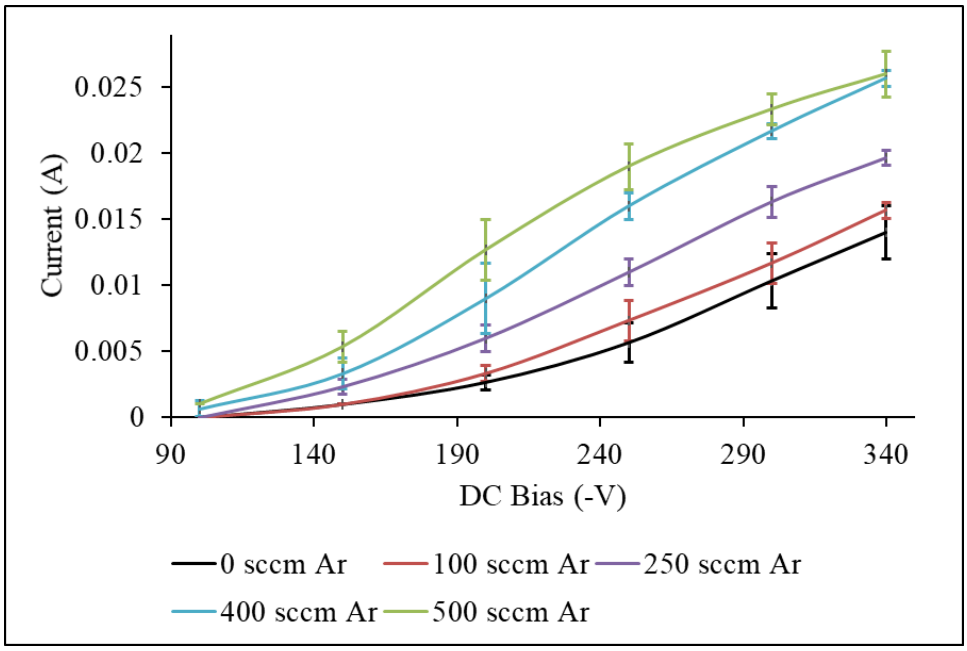

Fig 15: Current against bias voltage for different argon flow at 30 torr.

At 10 and 20 torr, there is a peak in current for varying argon flow rate at voltage below – 150V. However, at 30 torr, there is no peak in current. This effect will be used in BEN of boron rich materials to pretreat a silicon substrate. This effect will also be explained in the discussion section.

3.1.2 Nucleation Density

At 10 and 20 torr, there is a peak in current at 100 sccm and 250 sccm argon flow respectively for DC bias – 250 V. However, there is no peak in current at 30 torr. The experiments were repeated 5 times to test for reproducibility and the average result is displayed in Fig. 16. The error bars are the standard deviation of the results.

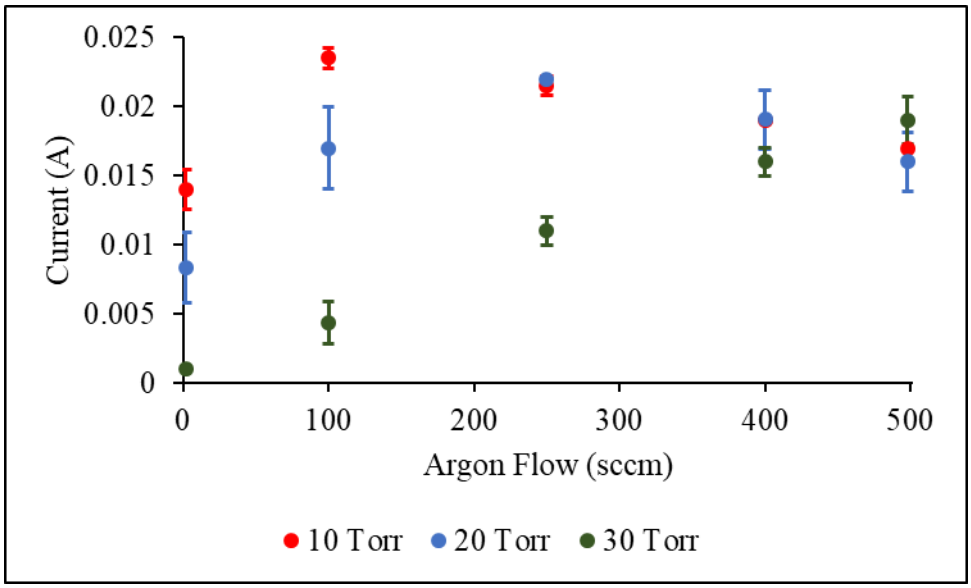

Fig. 16: Current against argon flow at – 250 V DC bias

In order to investigate the effects of DC bias and argon in the plasma on nucleation density, four experiments were carried out at 10 torr (labelled 1 – 4), at 20 torr (labelled 5 – 8), and at 30 torr (labelled 9 – 12), as summarized in Table 1. In experiment 1, 5, and 9, Ar is used in an H_2 plasma prior to nucleation from B_2H_6 on a negatively biased substrate at their respective pressure. Experiments 2, 6, and 10 serve as controls (no DC bias) in order to evaluate the effect of DC bias on nucleation density. Experiments 3, 7, and 11 serve as controls (no Ar) in order to evaluate the effect that Ar sputtering has on the silicon substrate surface roughness prior to nucleation. Experiments 4, 8, and 12 serve as controls (no Ar or DC bias) in order to evaluate the effect that both Ar and DC bias have on nucleation density.

Pressure (torr)	Label	Ar Flow (sccm)	DC Bias (-V)	Nucleation Density (mm^{-2})	T_s (°C)	Fig
10	1	100	250	2×10^6	700 ± 10	18 (a)
	2	100	0	4×10^4	690 ± 10	18 (b)
	3	0	250	2×10^5	700 ± 2	18 (c)
	4	0	0	1×10^4	690 ± 30	18 (d)
20	5	100	250	2×10^6	830 ± 5	19 (a)
	6	100	0	1×10^4	770 ± 10	19 (b)
	7	0	250	2×10^5	850 ± 10	19 (c)
	8	0	0	2×10^4	740 ± 2	19 (d)
30	9	100	250	3×10^5	920 ± 2	20 (a)
	10	100	0	1×10^5	960 ± 10	20 (b)
	11	0	250	2×10^5	920 ± 10	20 (c)
	12	0	0	5×10^4	960 ± 3	20 (d)

Table 1: Nucleation density results. The highest nucleation density at each pressure occurs when the silicon substrate is exposed to Ar/H_2 plasma with a DC bias. The lowest nucleation density occurs when the silicon substrate is neither exposed to Ar nor to a DC bias prior to nucleation.

During nucleation, the hydrogen and diborane flow rates are kept at 500 sccm and 2 sccm respectively. Therefore, N is kept constant during the 12 results shown. When a DC bias is used, ions are accelerated towards the negatively charged substrate, and thus K increases. Therefore, when only the DC bias changes between experiments, such as between experiment 1 and 2, or 3 and 4, and so on, the nucleation density increases.

Argon can be used to sputter silicon [22, 23]. This increases the surface roughness of the silicon substrate and W_{net}^{*} decreases. Therefore, when argon is used in the plasma prior to nucleation changes between experiments, such as experiment 1 and 3, or 2 and 4, and so on, the nucleation density increases. At 10 and 20 torr, the current flow through the silicon substrate is higher than at 30 torr. In this way, argon is more effective at sputtering the silicon substrate at 10 and 20 torr. We find that the nucleation density for experiments 1 and 5 are 10 × higher than the nucleation density for experiment 9.

Fig. 17 and 18 show images of different nucleation density at 10 torr. In Fig 17, the binary image is shown where the black background represents the silicon substrate, and the white dots represents the nucleation. In fig 18, the original image taken by camera on optical microscopy is shown. The original image is converted into binary image to be analyzed for nucleation density.

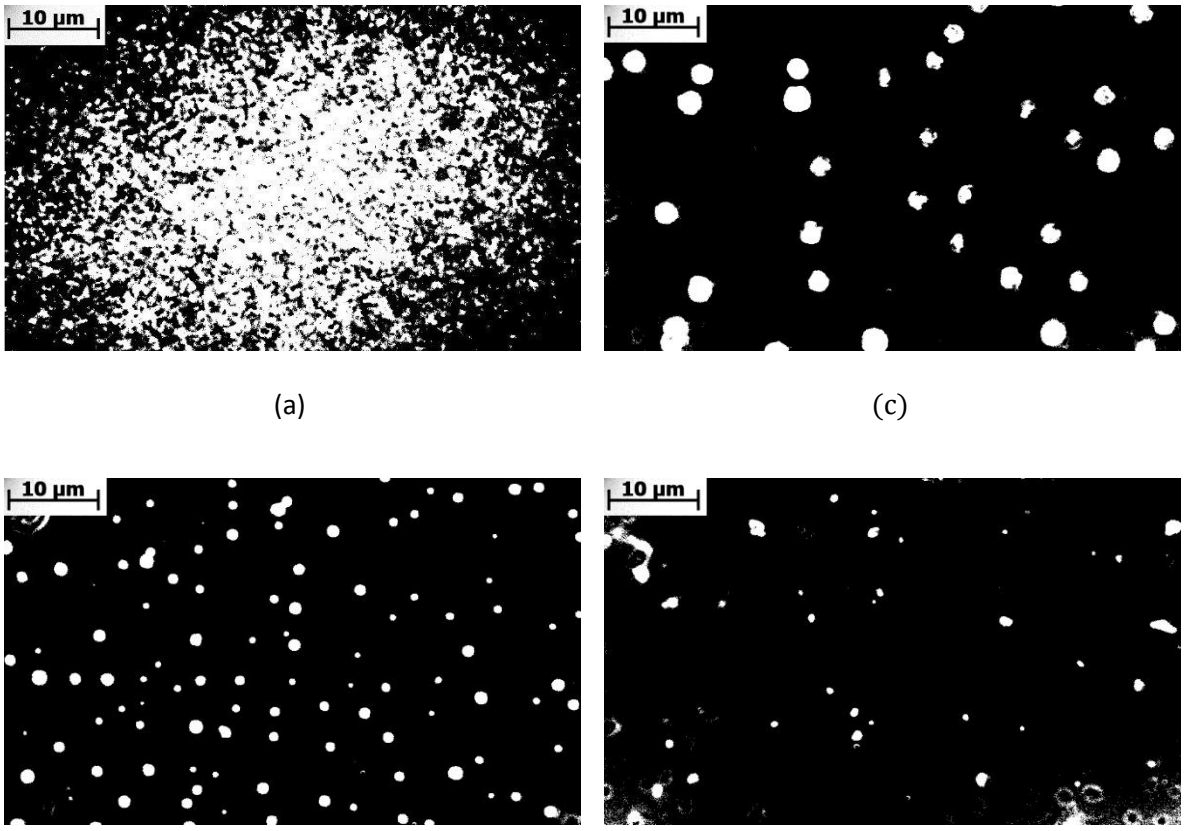

Fig. 17: Binary image of nucleation at 10 torr. (a) Experiment 1, (b) experiment 2, (c), experiment 3 and (d) experiment 4.

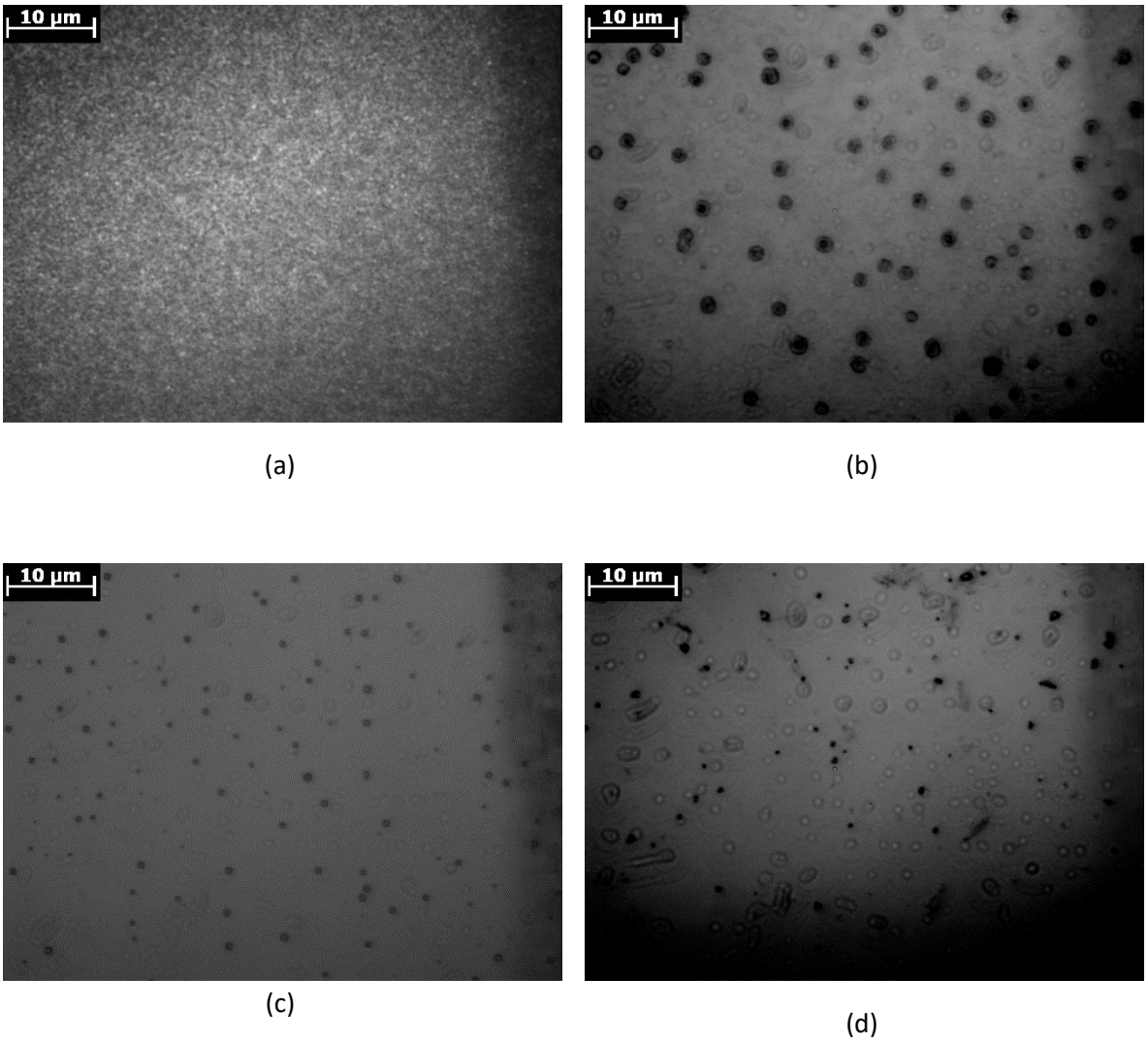

Fig. 18: Original image of nucleation at 10 torr. (a) Experiment 1, (b) experiment 2, (c), experiment 3 and (d) experiment 4.

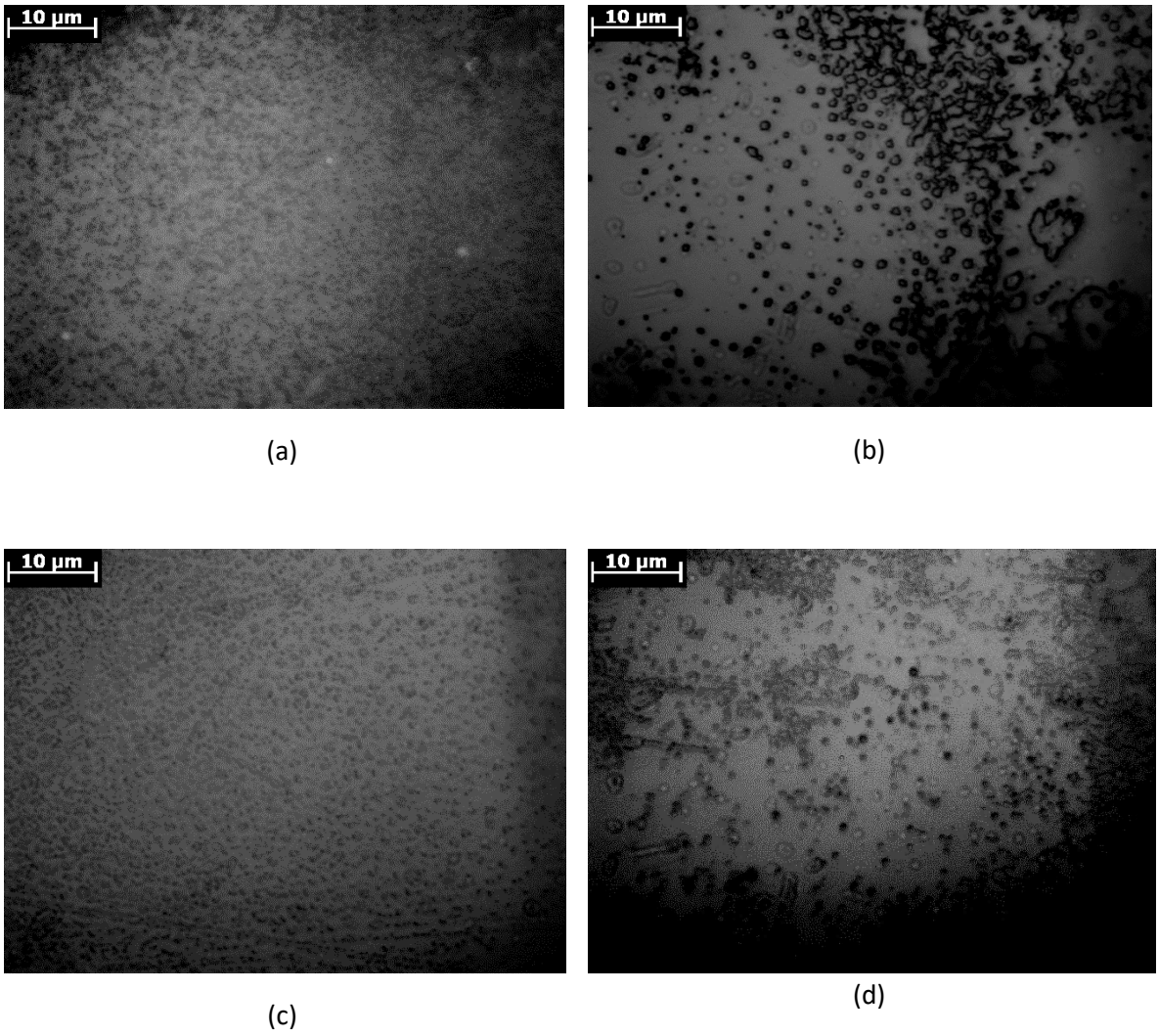

Fig. 19: Original image nucleation at 20 torr. (a) Experiment 5, (b) experiment 6, (c), experiment 7 and (d) experiment 8.

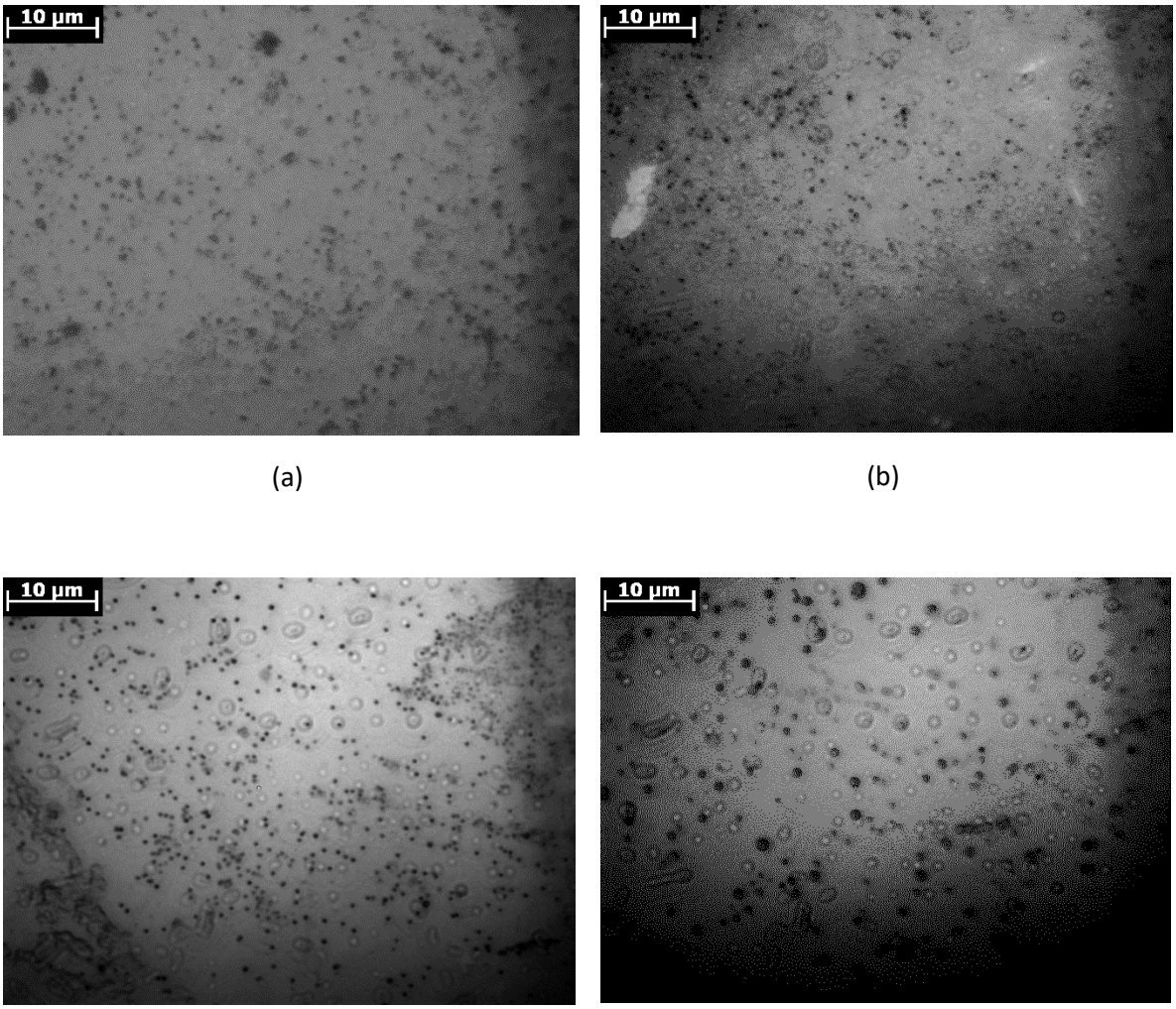

Fig. 20: Original image of nucleation at 30 torr. (a) Experiment 9, (b) experiment 10, (c), experiment 11 and (d) experiment 12.

3.1.3 X-ray Photoelectron Spectroscopy

X-ray Photoelectron Spectroscopy (XPS) is used for chemical analysis of the surface where materials are nucleated. This is done by irradiating the nucleated substrate with x-rays and analyzing the energy of the detected electrons emitted by the photo electric effect. The emitted electrons have kinetic energy, EK, given by [24]:

$$EK = h\nu - BE - \phi \quad \text{..... [3]}$$

hν is the energy of the photon, BE is the binding energy of the atomic orbital from which electron originates, and ϕ is the work function specific surface of the material. Since each element has a unique set of binding energies, XPS can be used to identify and determine the concentration of elements present on the surface of the substrate.

XPS was used to analyze the most densely nucleated sample at each pressure. The nucleation was boron rich, 79% boron at 10 torr, 76% boron at 20 torr and 72% at 10 torr, as shown in Fig. 21.

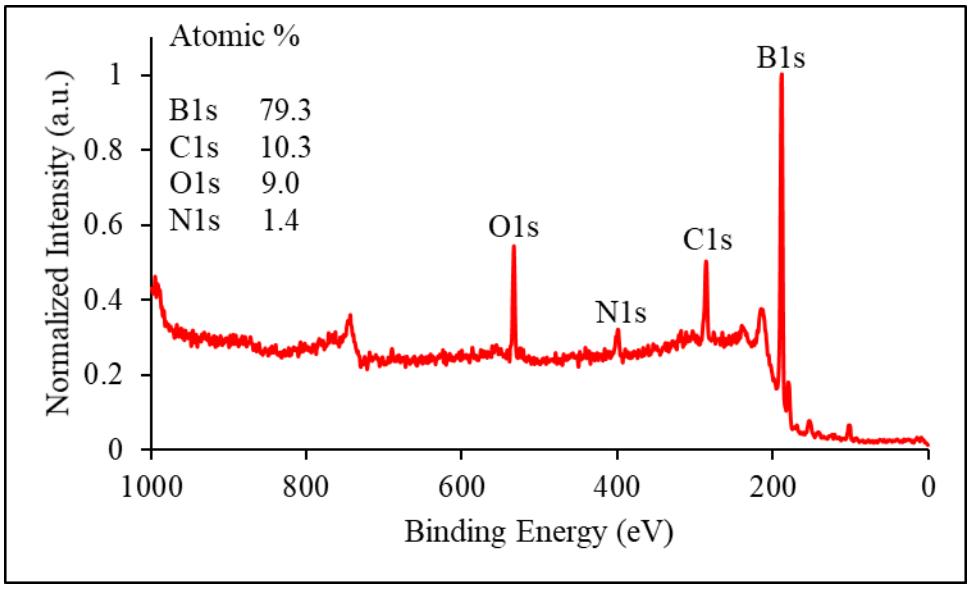
Atomic %
B1s 79.3
C1s 10.3
O1s 9.0
N1s 1.4
B1s
O1s
N1s
C1s
Normalized Intensity (a.u.)
0
0.2
0.4
0.6
0.8
1
1000
800
600
400
200
0
Binding Energy (eV)

(a)

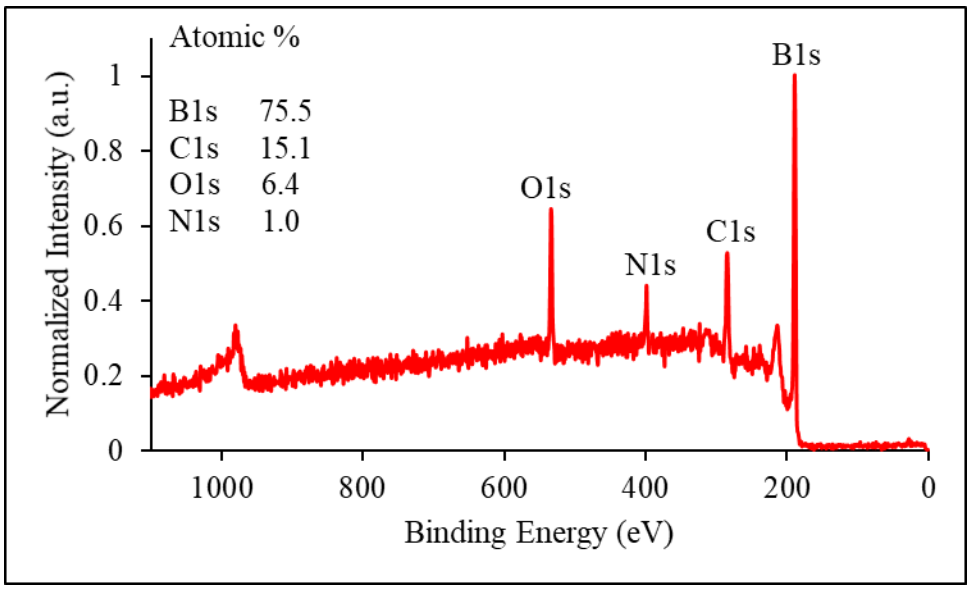
Atomic %
B1s 75.5
C1s 15.1
O1s 6.4
N1s 1.0
B1s
O1s
N1s
C1s
Normalized Intensity (a.u.)
0
0.2
0.4
0.6
0.8
1
1000
800
600
400
200
0
Binding Energy (eV)

(b)

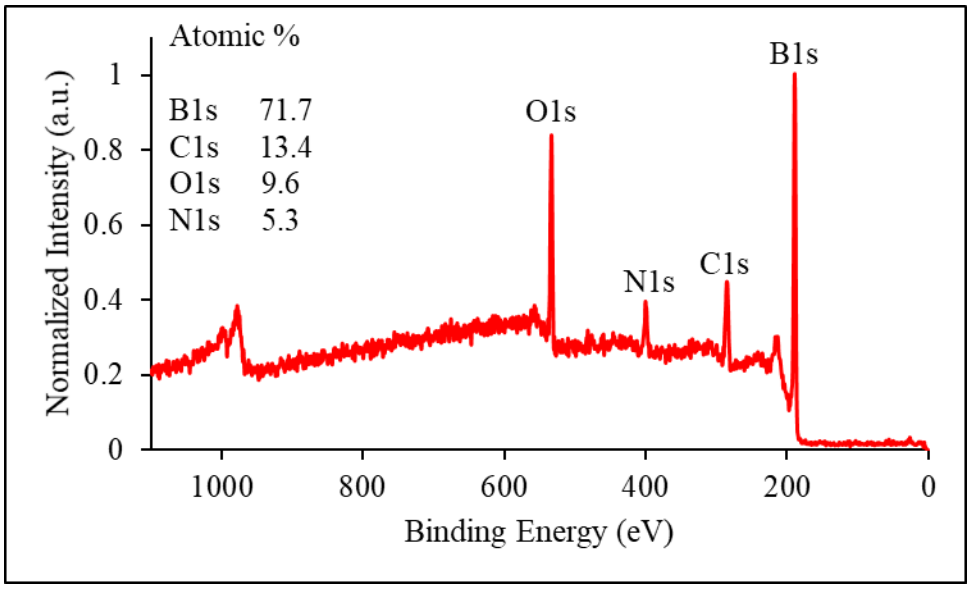

(c)

Fig. 21: XPS results of the most densely nucleated materials at each pressure. (a) 10 Torr (b) 20 Torr, (c) 30 Torr

3.2 Discussion

3.2.1 Substrate Temperature

The silicon substrate temperature is directly proportional to the ions bombarding the substrate per unit area [25]. The results of normalized substrate temperature against argon flow is shown in Fig. 22. The trend in how the substrate temperature varies is similar to how the current through the substrate varies. Therefore, the peak in current flow through the substrate is due to a peak in ions bombarding the substrate.

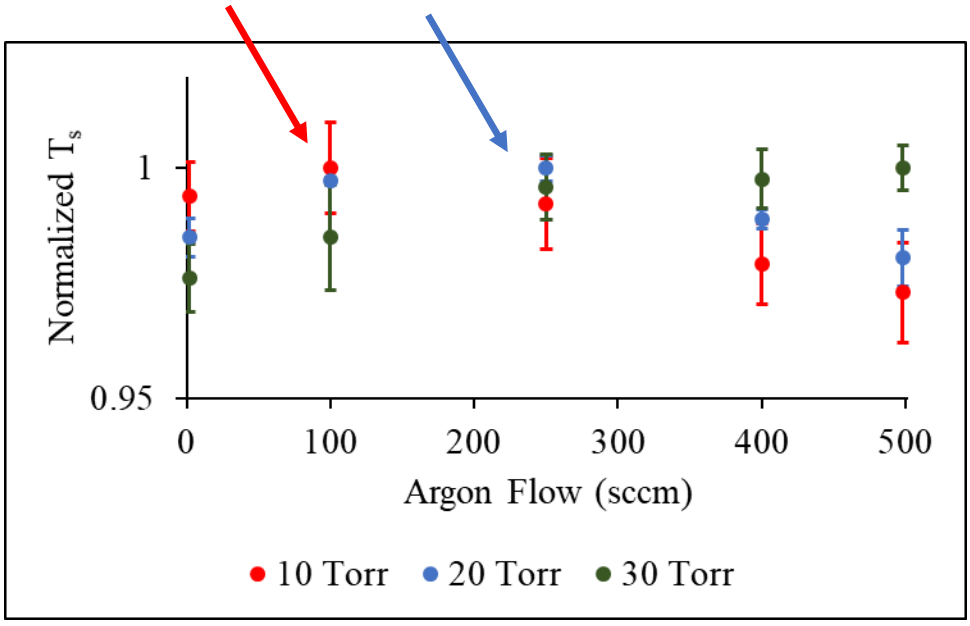

Fig. 22: Normalized substrate temp against argon flow. Peak in T_s at 10 and 20 torr is pointed by an arrow at each pressure.

T_s was recorded continuously during pre-treatment and nucleation. For example, the T_s of the 4 nucleation are shown in Fig. 23.

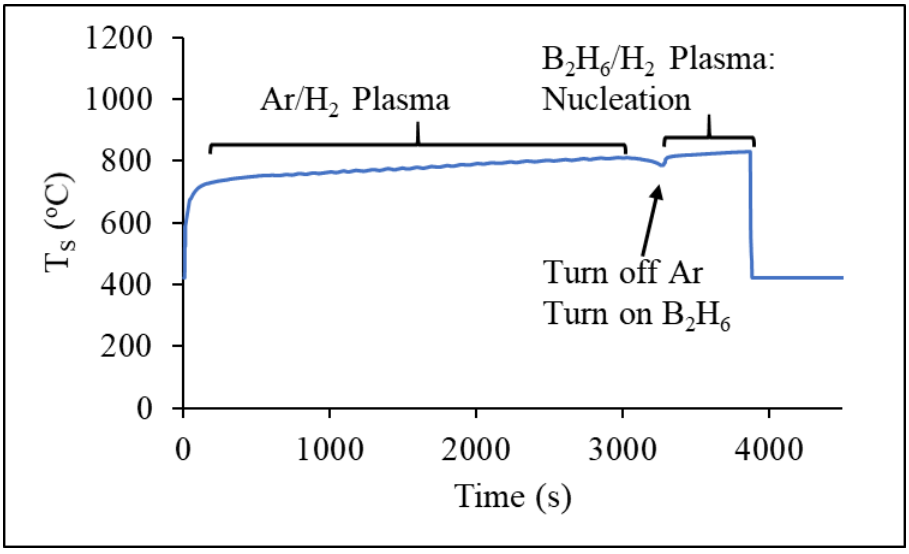

(a)

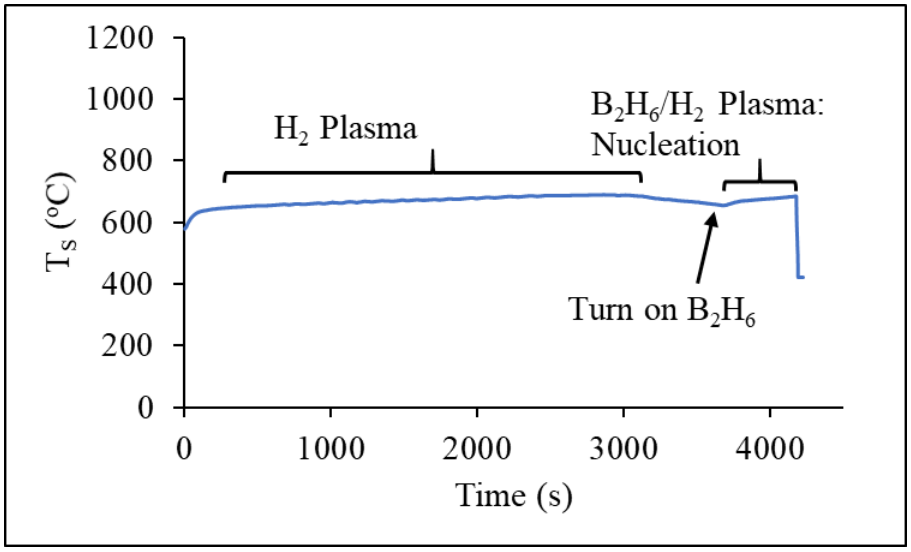
1200
1000
800
600
400
200
0
T_S (°C)
H_2 Plasma
B_2H_6/H_2 Plasma:
Nucleation
Turn on B_2H_6
0
1000
2000
3000
4000
Time (s)

(b)

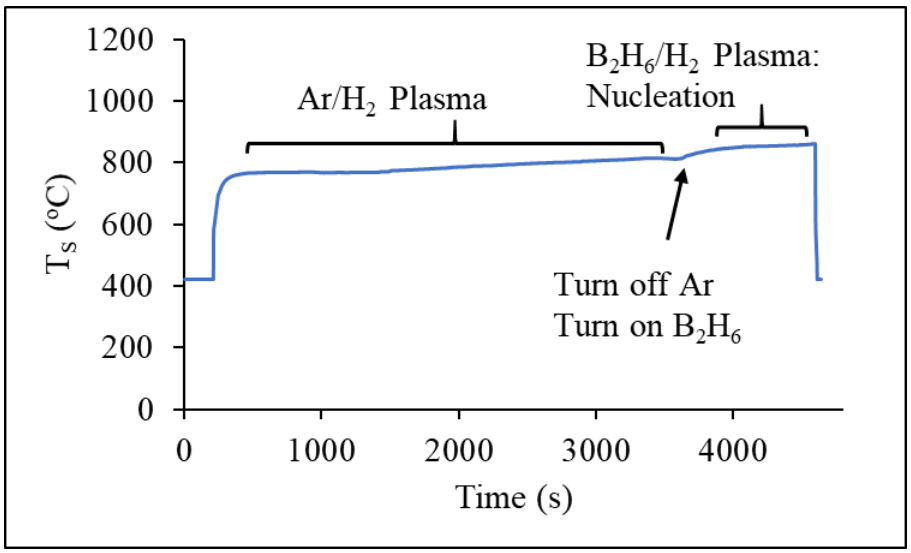
1200
1000
800
600
400
200
0
T_S (°C)
Ar/H_2 Plasma
B_2H_6/H_2 Plasma:
Nucleation
Turn off Ar
Turn on B_2H_6
0
1000
2000
3000
4000
Time (s)

(c)

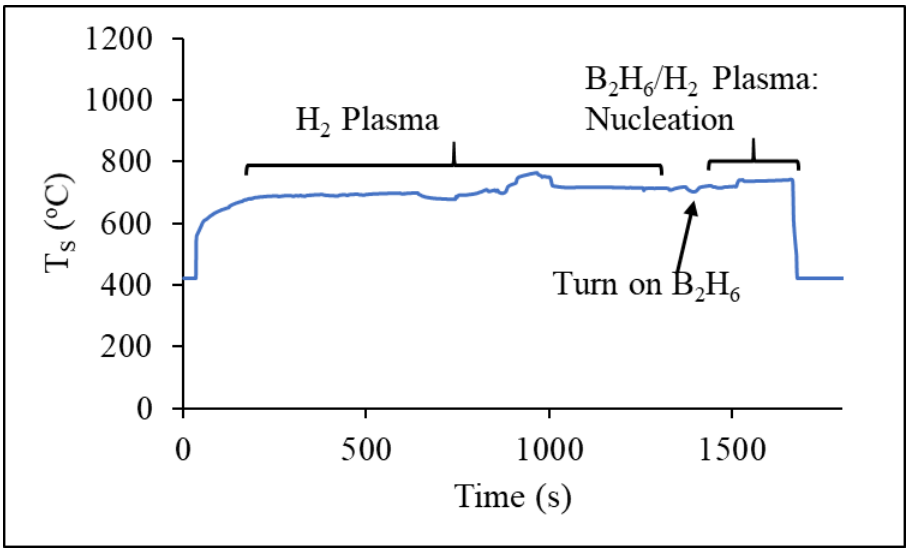

(d)

Fig 23: Example of T_s during nucleation. (a) Experiment 5, (b) Experiment 6, (c) Experiment 7 and (d) Experiment 8.

3.2.2 Electron Temperature

Using the Boltzmann plot, the electron temperature of the plasma [26] can be calculated from hydrogen [27] OES lines. This method only works when there is a local thermodynamic equilibrium (LTE). In literature, there are many instances where LTE was assumed in the microwave plasma in MPCVD, and hence the use of a Boltzmann plot was justified [28,29,30].

The electron temperature can be calculated according to the equation below:

$$\ln\left(\frac{I\lambda}{Ag}\right) = -\frac{1}{k_B T_e} E + C \quad \ldots\ldots\ldots\ldots [4]$$

I is the intensity of a hydrogen OES peak at a particular wavelength, λ. A and g, which are available on the NIST database are the transition probability for that particular excitation and the statistical weight of the excited (upper) state respectively [31]. E is the excitation energy. C is a constant, the y-intercept.

Here, 3 hydrogen peaks from the OES will be used for the Boltzmann plot, as listed in the table 2.

OES Peak	λ (nm)	$A_{ul}(\times 10^6\ s^{-1})$	g	E (eV)
H_γ	434	2.53	5	2.86
H_β	486	8.41	4	2.55
H_α	656	44.1	3	1.89

Table 2: Characteristics of hydrogen peaks for Boltzmann plot.

Graphs of Boltzmann plot at 10 torr are shown in Fig 24 and 25. Graphs of Boltzmann plot at 20 torr are shown in Fig 26 and 27. Boltzmann plot at 30 torr are shown in Fig 28 and 29. Table 3 shows all results of T_e according to Boltzmann plot.

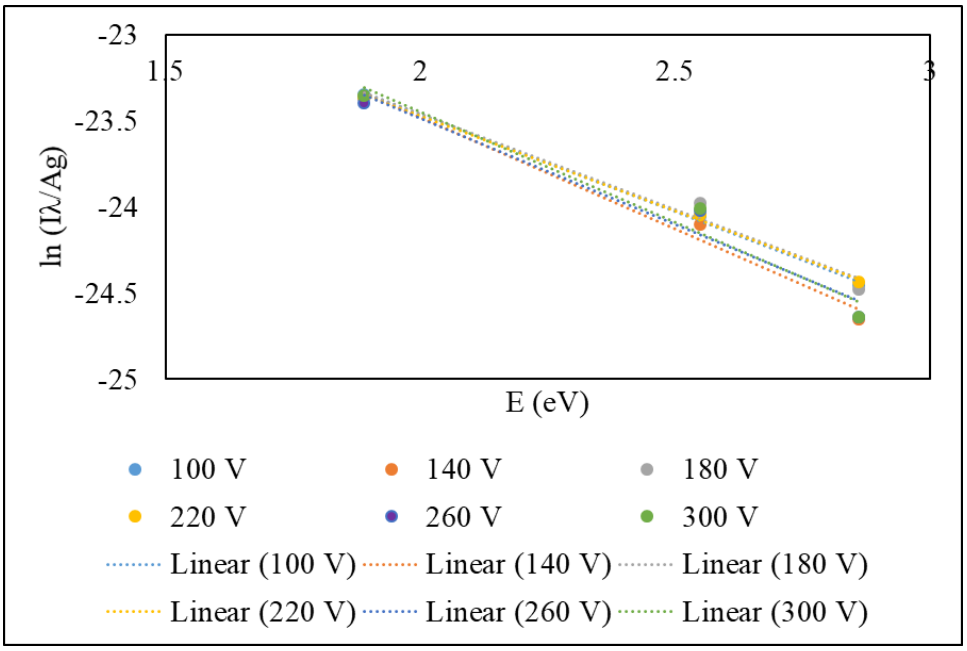

Fig 24: Boltzmann plot at 10 torr, 0 sccm

$T_e = 0.8 \pm 0.06$ eV

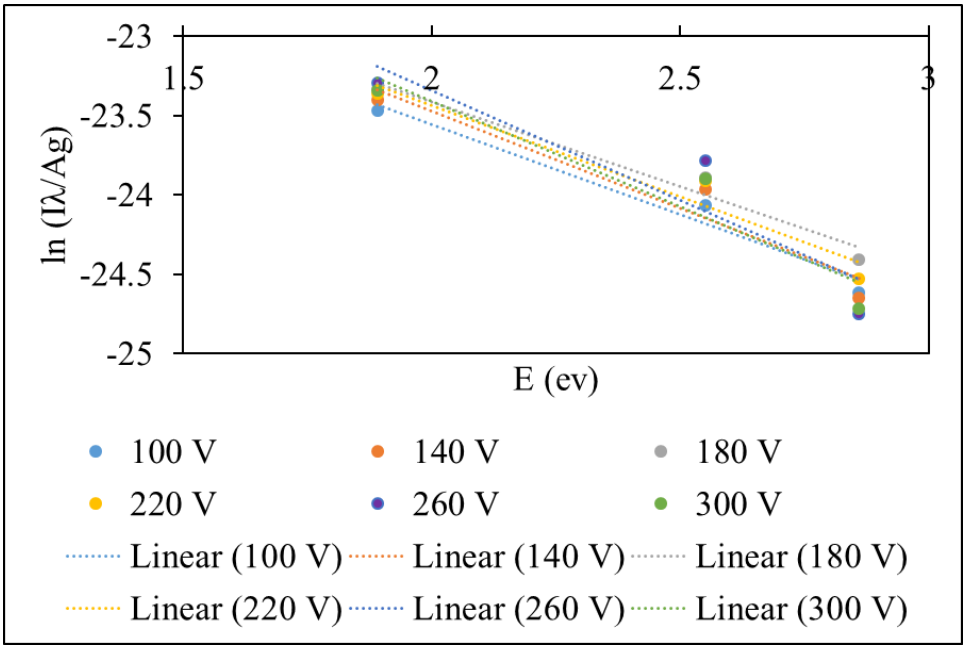

Fig 25: Boltzmann plot at 10 torr, 500 sccm

$T_e = 0.8 \pm 0.09$ eV

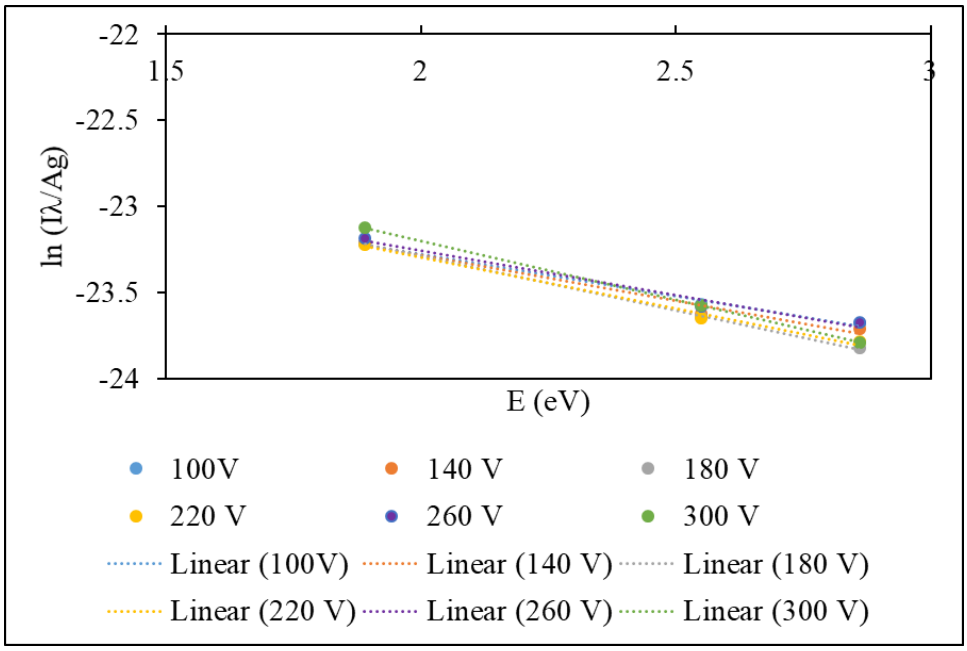

Fig 26: Boltzmann plot at 20 torr, 0 sccm
$T_e = 1.6 \pm 0.2$ eV

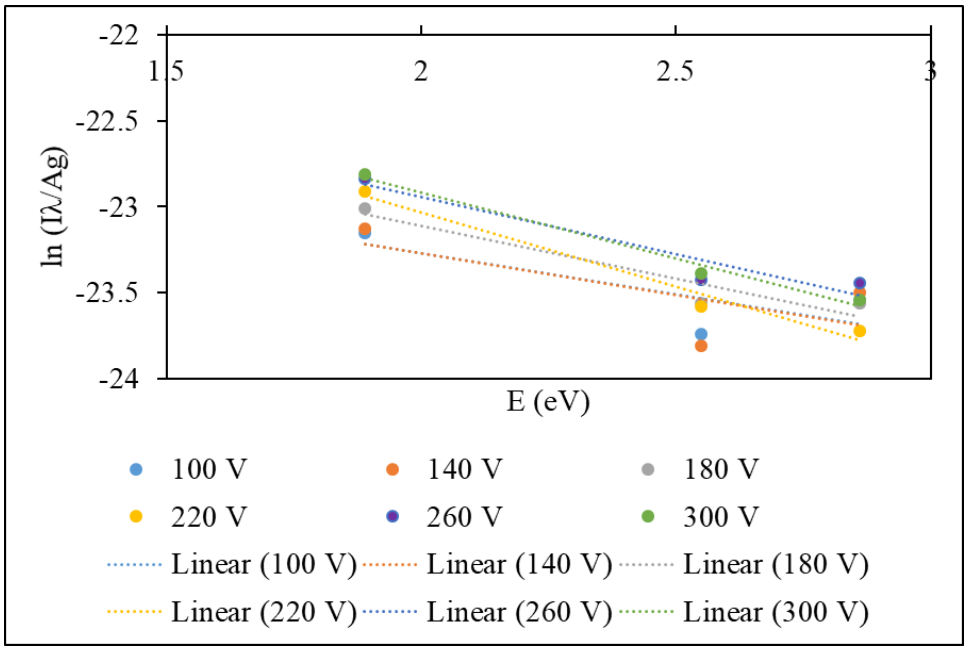

Fig 27: Boltzmann plot at 20 torr, 500 sccm
$T_e = 1.6 \pm 0.4$ eV

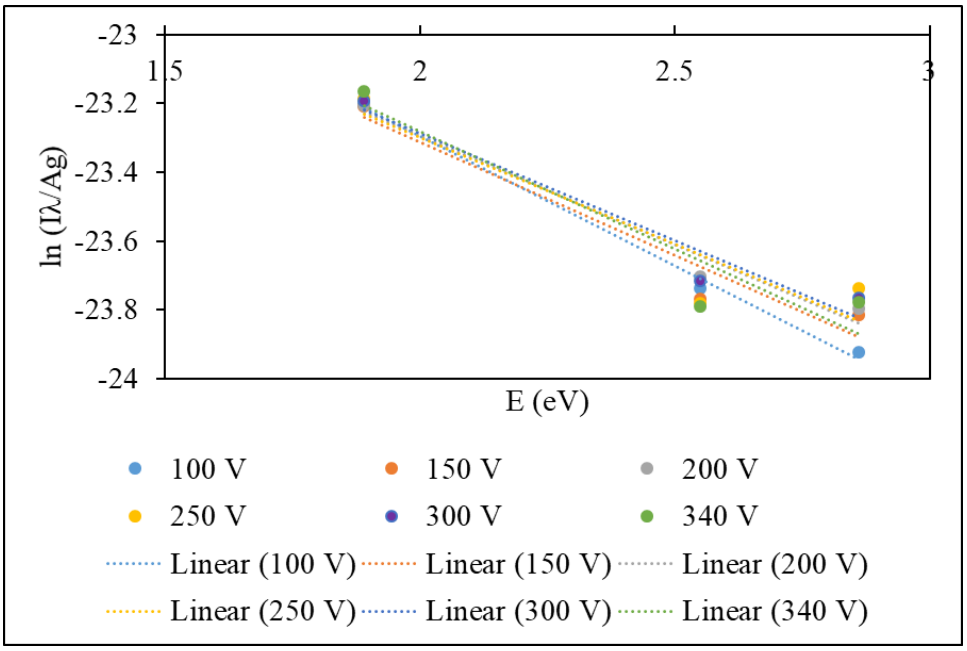

Fig 28: Boltzmann plot at 30 torr, 0 sccm
$T_e = 1.5 \pm 0.6$ eV

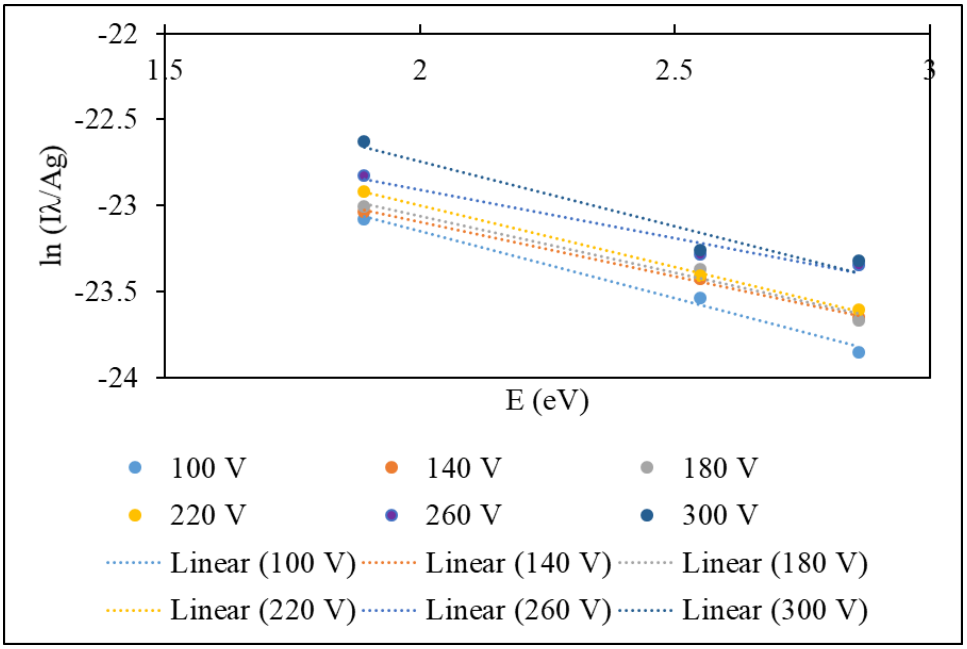

Fig 29: Boltzmann plot at 30 torr, 500 sccm
$T_e = 1.5 \pm 0.2$ eV

Pressure (Torr)	Ar Flow (sccm)	T_e (eV)
10	0	0.8 ± 0.06
	100	0.9 ± 0.03
	250	0.9 ± 0.07
	400	0.9 ± 0.04
	500	0.8 ± 0.09
20	0	1.6 ± 0.2
	100	1.6 ± 0.2
	250	1.4 ± 0.1
	400	1.5 ± 0.1
	500	1.6 ± 0.4
30	0	1.5 ± 0.6
	100	1.3 ± 0.1
	250	1.7 ± 0.2
	400	1.3 ± 0.1
	500	1.5 ± 0.2

Table 3: Results of T_e according to Boltzmann Plot

The ratio of intensities of H_α/H_β, plotted in Fig. 30, can also indicate the plasma T_e [32]. This method is suitable regardless of thermodynamic equilibrium. Quantitative values of the T_e are obtained using the following two equations [33].

$$\frac{I_{H\alpha}}{I_{H\beta}} = F\frac{k_e^{H\alpha}}{k_e^{H\beta}}\frac{v_{656}}{v_{486}}\,Q_{T,H} \text{ .....[5]}$$

$$Q_{T,H} = \frac{1+PT_e^{-\frac{1}{2}}\left[0.132\,\sigma_{\frac{H_\alpha}{H_2}}\chi_{H_2}+0.152\,\sigma_{\frac{H_\alpha}{H}}(1-\chi_{H_2})\right]}{PT_e^{-\frac{1}{2}}\left[0.426\,\sigma_{\frac{H_\beta}{H_2}}\chi_{H_2}+0.492\,\sigma_{\frac{H_\beta}{H}}(1-\chi_{H_2})\right]} \text{ ..... [6]}$$

$I_{H\alpha}$, and $I_{H\beta}$ are the emission intensity of H_α, and H_β respectively, measured using OES. F is an optical device factor [34,35]. $k_e^{H\alpha}$, and $k_e^{H\beta}$ are excitation rate constants for transitions H_2 $(n = 1) \rightarrow H$ $(n = 3)$, and $H(n = 1) \rightarrow H(n = 4)$ respectively [36]. v_{656}, and v_{486} are de-excitation frequency for H $(n = 3)$ and H $(n = 4)$ respectively [37]. n is the principle quantum number denoting energy level of electrons. P is the pressure in hecto-pascal and T_e is the electron temperature in Kelvin. $\sigma_{\frac{H_\alpha}{H_2}}$, and $\sigma_{\frac{H_\alpha}{H}}$ are quenching cross sections of H_α by H_2 molecules quenching cross sections of H_α by H atoms [35]. $\sigma_{\frac{H_\beta}{H_2}}$, and $\sigma_{\frac{H_\beta}{H}}$ are quenching cross sections of H_β by H_2 molecules and quenching cross sections of H_β by H atoms [37]. χ_{H_2} is the mole fraction of the H_2. The optical device factor is not calculated here. Instead, a normalized plot of T_e to T_e at 30 torr (T_{e30}) is plotted for 10 (T_{e10}) and 20 (T_{e20}) torr in Fig 31.

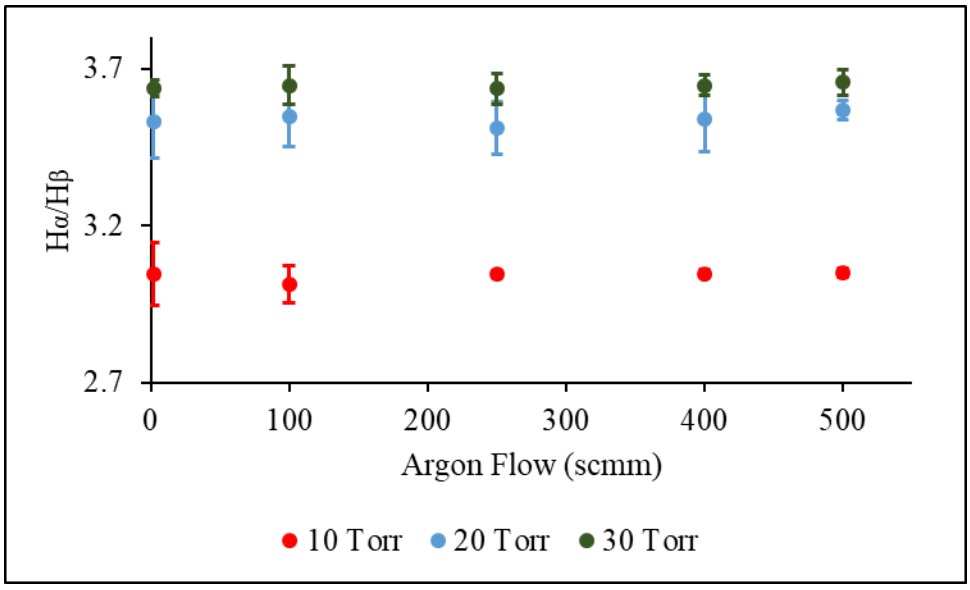

Fig. 30: Ratio of H_α to H_β is constant at each pressure.

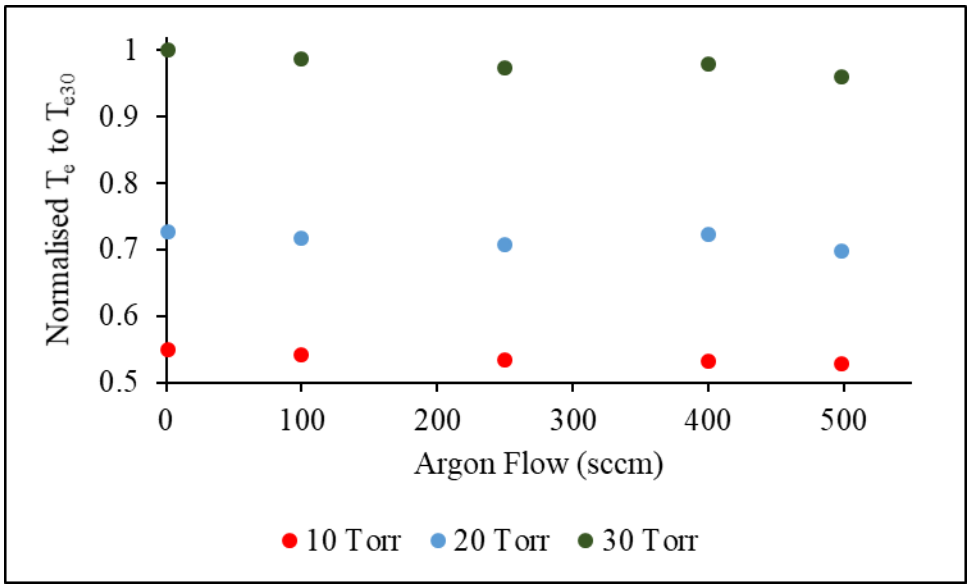

Fig 31: T_e, normalized in terms of units of T_{e30}.

T_{e10} is about $0.54T_{e30}$, and T_{e20} is about $0.7T_{e30}$.

Different OES were taken of the plasma from the initial OES during experiment. These new OES were used to calculate T_e, and each $H_\alpha$and H_β peak was scanned individually. The intensity of the peak was used to calculate T_e according to eq. 5 and eq. 6.

3.2.3 Plasma Volume

The plasma is cold and thus follows ideal gas law [20, 21]. When the pressure and the electron temperature of the plasma are kept constant, adding argon to the plasma should increase the volume. Photographs of plasma and their related image intensity have been used in literature to show plasma volume [38, 39]. Here, a photo of the plasma is taken for the different flow rates of argon and at different pressure, from a constant angle and camera setting, as shown in Fig. 32. The image intensity of the plasma is analyzed right above the substrate by calculating the mean grey value of the image using ImageJ. In Fig. 33, the normalized value of the image intensity of the plasma at each pressure is plotted. The changes in image intensity indicates changes in the volume of the plasma. The decrease in intensity at 10 and 20 torr with increased flow rate of argon indicates that the plasma volume is increasing. Therefore, ions are spread out over a larger volume. However, at 30 torr, there does not seem to be an increase in plasma volume with varied flow rate of argon. At higher pressure the mean free path of the plasma decreases.

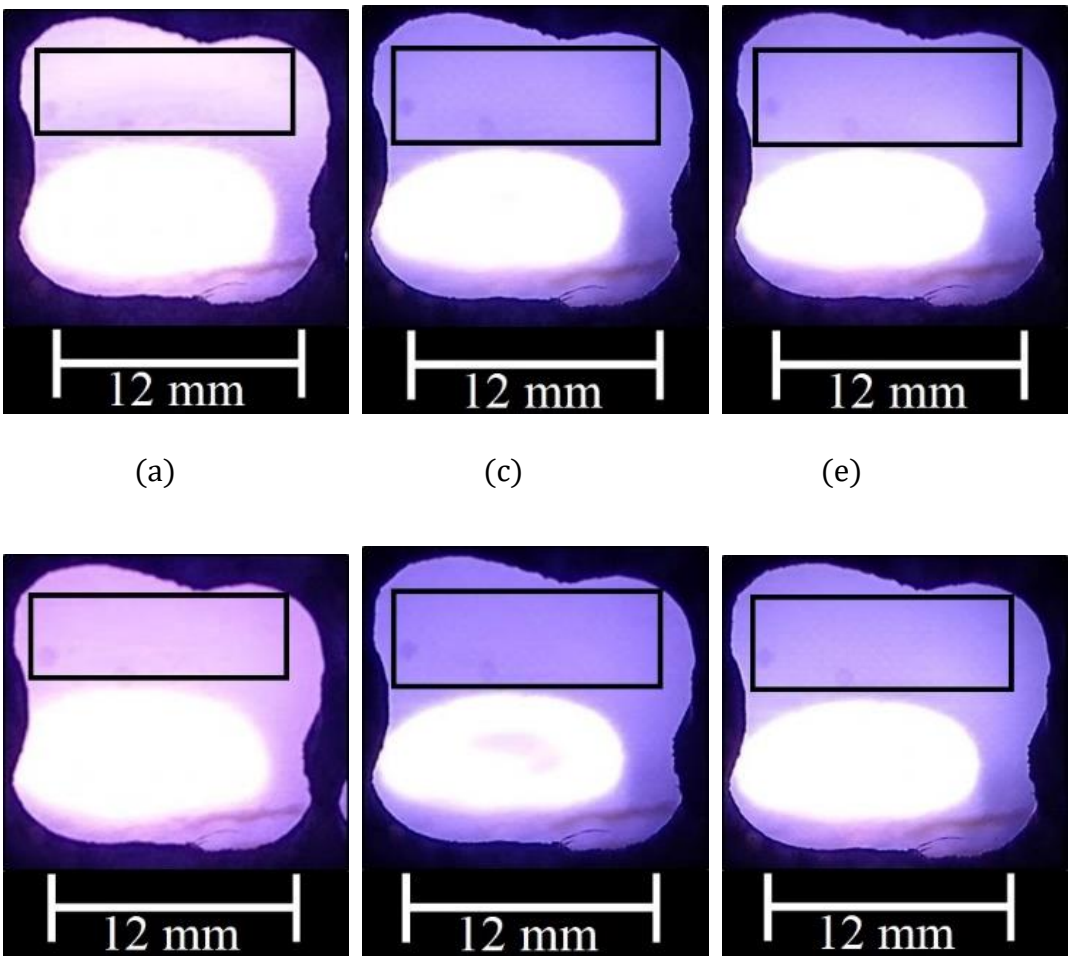

(a) (c) (e)

(b) (d) (f)

Fig. 32: Plasma above substrate.

(a) 500 sccm H_2, 0 sccm Ar, 10 Torr. (b) 500 sccm H_2, 500 sccm Ar, 10 Torr. (c) 500 sccm H_2, 0 sccm Ar, 20 Torr. (d) 500 sccm H_2, 500 sccm Ar, 20 Torr. (e) 500 sccm H_2, 0 sccm Ar, 30 Torr. (f) 500 sccm H_2, 500 sccm Ar, 30 Torr.

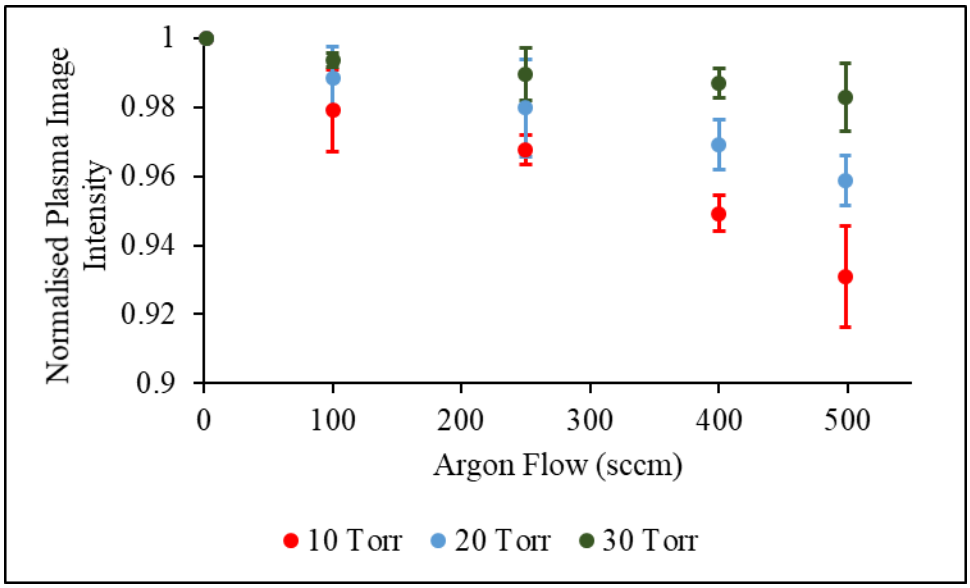

Fig. 33: Normalized image intensity of plasma above silicon substrate.

Ar flow varies at -250V DC bias

When the silicon substrate holder is negatively biased and the chamber of the CVD is grounded, as is the case in this set up, the electric field decreases away from the plasma [40]. As the plasma volume increases at 10 and 20 torr, more ions are spread away from the negatively charged substrate. Hence, these ions bombard the silicon substrate at a lower rate. This leads to a decrease in current flowing through the substrate due to ion bombardment. At 30 torr, the plasma volume does not increase compared to 10 and 20 torr. Therefore, the rate at which ions bombard the silicon substrate does not decrease, and hence there is no decrease in current with increased argon flow.

Chapter 4: CONCLUSIONS

4.1 DC Bias

A DC Bias was implemented in the CVD which can create an electric field between the anode (substrate) and the cathode (CVD chamber). This field directs ions towards the substrate leading to ion bombardment. This is a current that flows through the silicon substrate which can be recorded. This current varies as the amount of Ar in an H_2 plasma changes such that there is a peak at 10 and 20 torr. This peak in current due to ion bombardment is also reflected in T_s since the latter is directly proportional to ion bombardment. Results of OES intensity shows that the electric field due to the DC Bias does not affect any particular line intensity.

4.2 Nucleation

MPCVD with DC bias was optimized for highest current flow through a silicon substrate due to an Ar/H_2 plasma at 10 torr. This current was analysed for several argon flow rates between 0 and 500 sccm. Using the results found at 10 torr, silicon substrates were pre-treated with the DC bias in an Ar/H_2 plasma. Heterogenous nucleation density was enhanced for boron-rich materials. Control experiments were performed to evaluate the individual effect of using a DC bias and/or argon in the plasma. The result of nucleation density shows that nucleation density was 200 times higher when a silicon

substrate was exposed to Ar/H_2 plasma with DC bias than when the substrate was not exposed to Ar/H_2 plasma and DC bias. Nucleation density was also tested at 20 and 30 torr in order to evaluate the effect of pressure on the nucleation density while keeping other experimental parameters constant. At 20 and 30 torr, the nucleation density was 100 times, and 6 times higher when a silicon substrate was exposed to Ar/H_2 plasma with DC bias than when the substrate was not exposed to Ar/H_2 plasma and DC bias. While BEN has been commonly reported for carbon-based coatings, these results demonstrate that BEN would be effective to synthesize boron-rich materials using MPCVD.

4.3 Future Directions

In this work, during the calculation of T_e using $\frac{H_\alpha}{H_\beta}$, F was assumed to be a constant. This allowed the calculation to show how T_e changes with Ar flow and pressure. F can be calculated by studying reference [35]. F is shown to vary with how the optical device (i.e. optical emission spectrometer) responds to the intensity of Ar and H light travels through. Therefore, F need to be calculated for each lab's OES setup. This can allow a student to calculate exact T_e. Knowing F can also allow a student to calculate gas temperature by analysing the intensity of argon and hydrogen in the plasma. Rotational temperature of the plasma can also be calculated by analysing the Q-branch on a Boltzmann plot. Fig 34 shows wavelength 600 nm to 620 nm from Fig 3. The Q-branch is visible and labelled. However, an individual OES scan is needed to get better resolution. Table 4 lists the Q-branch wavelength [41].

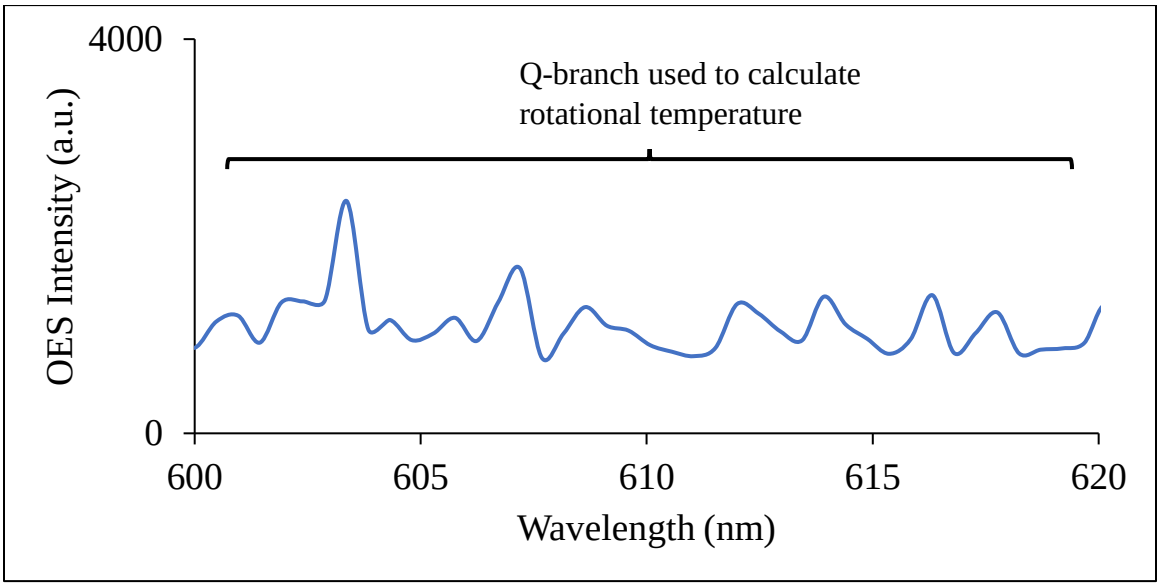

Fig 34: Q-branch from Fig. 3. The resolution can be improved by future student.

Q-branch	Wavelength (nm)
Q_1	601.83
Q_2	602.38
Q_3	603.19
Q_4	604.27
Q_5	605.61
Q_6	607.20
Q_7	609.04
Q_8	611.11
Q_9	613.41
Q_{10}	615.93

Table 4: Listing the Q-branch values.

LIST OF REFERENCES

[1] D.J. Kester, R. Meisser, Phase control of cubic boron nitride thin films, J. Appl. Phys. 72 (1992) 504 – 13. https://doi.org/10.1063/1.351881

[2] S.N. Monteiro, A.L.D. Skury, M. Giardinieri de Azevedo, G.S. Bobrovnitchii, Cubic boron nitride competing with diamond as a superhard engineering material – an overview, Journal of Materials Research and Technology, 2(1), 68 – 74, 2013. https://doi.org/10.1016/j.jmrt.2013.03.004

[3] A.R. Oganov, V.L. Solozhenko, Boron: a Hunt for Superhard Polymorphs, arXiv, 2009. https://arxiv.org/ftp/arxiv/papers/0911/0911.3193.pdf

[4] S. Veprek, R.F. Zhang, A.S. Argon, Mechanical Properties and Hardness of Boron and Boron Rich Solids, J. Superhard Mater. 33 (2011) 60 – 74. https://doi.org/10.3103/S1063457612060068

[5] D.R. Tallant, T.L. Aselage, A.N. Campbell, D. Emin, Boron Carbides structure by Raman Spectroscopy, Phys. Rev. B. 40 (1989) 5649 – 56. http://dx.doi.org/10.1103/physrevb.40.5649

[6] A.K. Suri, C. Subramanian, J.K. Sonber, T.S.R. Ch. Murthy, Synthesis and consolidation of boron carbide: a review, Int. Mater. Rev. 55 (2010) 4 – 40. https://doi.org/10.1179/095066009X12506721665211

[7] V. L. Solozhenko, O. O. Kurakevych, D. Andrault, Y. L. Godec, M. Mezouar, Ultimate Metastable Solubility of Boron in Diamond: Synthesis of Superhard Diamondlike BC5, Phys. Rev. Lett. 102 (2009) 179901. https://doi.org/10.1103/PhysRevLett.102.015506

[8] J.C. Arnault, L. Demuynck, C. Speisser, F. Le Normand, Mechanisms of CVD diamond nucleation and growth on mechanically scratched Si(100) surfaces, Eur. Phys. J. B. 11 (1999) 327 – 343. https://doi.org/10.1007/s100510050943

[9] J.L. Davidson, C. Elllis, and R. Ramesham, Selective Deposition of Diamond Films, J. Electron. Mater. 18 (1989) 711 – 5. https://doi.org/10.1007/BF02657523

[10] S. Yugo, T. Kanai, T. Kimura, T. Muto, Generation of diamond nuclei by electric field in plasma chemical vapor deposition, Appl. Phys. Lett. 58 (1991) 1036 – 8. https://doi.org/10.1063/1.104415

[11] B.B. Wang, W.L. Wang, K.J. Liao, Theoretical analysis of ion bombardment roles in the bias-enhanced nucleation process of CVD diamond, Diamond Relat. Mater. 10 (2001) 1622 – 26. https://doi.org/10.1016/S0925-9635(01)00435-6

[12] B.R. Stoner, G.-H. M. Ma, S.D. Wolter, J.T. Glass, Characterization of bias-enhanced nucleation of diamond on silicon by invacuo surface analysis and transmission electron microscopy, Phys. Rev. B. 45 (1992) 11067 – 84. https://doi.org/10.1103/PhysRevB.45.11067

[13] M. Kuhr, S. Reinke, W. Kulisch, Nucleation of cubic boron nitride (c-BN) with ion-induced plasma-enhanced CVD, Diamond Relat. Mater. 4 (1995) 375 – 80. https://doi.org/10.1016/0925-9635(94)05310-3

[14] K. Kelton, A. Greer, Nucleation in Condensed Matter, Volume 15, Pergamon Material Series

[15] A. Menendez, R. Pereiro, N. Bordel, A. Sanz-Medel, H2/Ar direct current glow discharge mass spectrometry at constant voltage and pressure, Spectrochimica Acta Part B 60 (2005) 824 – 33. https://doi.org/10.1016/j.sab.2005.06.001

[16] S. Sivaram, Chemical Vapor Deposition: Thermal and Plasma Deposition of Electronic Materials, Springer Science Business Media, New York

[17] C.A. Schneider, W.S. Rasband, K.W. Eliceiri, NIH Image to ImageJ: 25 years of image analysis, Nat. methods. 2012; 9: 671 – 5. https://doi.org/10.1038/nmeth.2089

[18] J. Schindelin, I. Arganda-Carreras, E. Frise, V. Kaynig, M. Longair, T. Pietzsch, S. Preibisch, C. Rueden, S. Saalfeld, B. Schmid, J. -Y. Tinevez, D. J. White, V. Hartenstein, K. Eliceiri, P. Tomancak, A. Cardona, Fiji: an open-source platform for biological-image analysis, Nat. Methods. 2012; 9: 676 – 82. https://doi.org/10.1038/nmeth.2019

[19] T. Kuo, J. Byun, ITCN: Image-based Tool for Counting Nuclei, Center for Bio-image Informatics at UC Santa Barbara https://imagej.nih.gov/ij/plugins/itcn.html (accessed 21 Mar 2020)

[20] Stuart M. Leeds, PhD Thesis, University of Bristol, June 1999 http://www.chm.bris.ac.uk/pt/diamond/stuthesis/chapter5.htm#_edn3 Accessed (20 Oct 2019)

[21] K. Wiesemann, A Short Introduction to Plasma Physics, arXiv, https://arxiv.org/ftp/arxiv/papers/1404/1404.0509.pdf

[22] P.C. Zalm, Energy dependence of the sputtering yield of silicon bombarded with neon, argon, krypton, and xenon ions, J. Appl. Phys. 54 (1983) 2660 – 6. https://doi.org/10.1063/1.332340

[23] M.P. Seah, T.S. Nunney, Sputtering yields of compounds using argon ions, J. Appl. Phys. 43 (2010) 253001 – 13. https://doi.org/10.1088/0022-3727/43/25/253001

[24] J. F. Moulder, W.F. Stickle, P.E. Sobol, and K.D. Bomben, Handbook of X-ray Photoelectron Spectroscopy, Perkin – Elmer Corporation, Eden Prairie, Minnesota, USA.

[25] Y. Wada, H. Usui, M. Ashikawa, Substrate Temperature Measurement during Ion Implantation, Jpn. J. Appl. Phys. 14 (1975) 1351 – 56. https://doi.org/10.1143/JJAP.14.1351

[26] J. Zalach, St. Franke, Iterative Boltzmann plot method for temperature and pressure determination in a xenon high pressure discharge lamp, J. Appl. Phys. 113 (2013) 1 – 7. https://doi.org/10.1063/1.4788701

[27] N. Guohua, Z. Peng, C. Cheng, S. Ye, T. Hirotaka, M. Yuedong, Characterization of a steam plasma jet at atmospheric pressure, Plasma Sources Sci. Technol. 21 (2012): 1 – 12. https://doi.org/10.1088/0963-0252/21/1/015009

[28] G. Shivkumar, S.S. Tholeti, M.A. Alrefae, T.S. Fisher, A.A. Alexeenko, Analysis of hydrogen plasma in a microwave plasma chemical vapor deposition reactor, J. Appl. Phys. 119 (2016) 11301 https://doi.org/10.1063/1.4943025

[29] K.W. Hemawan, R.J. Hemley, Optical emission diagnostics of plasmas in chemical vapor deposition of single crystal diamond, J. Vac. Sci. Technol., A, 33 (2015) 061302. https://doi.org/10.1116/1.4928031

[30] H. Jia, H. Kuraseko, M. Kondo, A microwave-induced plasma source: Characterization and application for the fast deposition of crystalline silicon films, J. Appl. Phys. 103 (2008) 024904. https://doi.org/10.1063/1.2833339

[31] V.K. Shen, D.W. Siderius, W.P. Krekelberg, H.W. Hatch, NIST Standard Reference Simulation Website, NIST Standard Reference Database Number 173, National Institute of Standards and Technology, Gaithersburg MD, 20899, http://doi.org/10.18434/T4M88Q , (retrieved <31 Aug 2019>)

[32] C. Park, Hydrogen line ratios as electron temperature indicators in nonequilibrium plasmas, Quant. Spectrosc. Radiat. Transfer. 12 (1972) 323 – 70. https://doi.org/10.1016/0022-4073(72)90050-7

[33] A. Gicquel, N. Derkaoui, C. Rond, F. Benedic, G. Cicala, D. Moneger, K. Hassouni, Quantitative analysis of diamond deposition reactor efficiency, Chem. Phys. 398 (2012) 239 – 47. https://doi.org/10.1016/j.chemphys.2011.08.022

[34] K. Pashova, I. Hinkov, X. Aubert, S. Prasanna, F. Benedic, S. Farhat, Graphene synthesis by microwave plasma chemical vapor deposition: analysis of the emission spectra and modeling, Plasma Sources Sci. Technol. 28, (2019) 045001 – 18. https://doi.org/10.1088/1361-6595/ab0b33

[35] A. Gicquel, M. Chenevier,Kh. Hassouni, A. Tserepi, M. Dubus, Validation of actinometry for estimating relative hydrogen atom densities and electron energy evolution in plasma assisted diamond deposition reactors, J. Appl. Phys. 83 (1998) 7504 - 21. https://doi.org/10.1063/1.367514

[36] R.K. Janev, Elementary Process in Hydrogen Plasma, Springer Berlin, 1987. https://doi.org/10.1002/ctpp.2150290103

[37] S. Lauer, H. Liebel, F. Vollweiler, O. Wilhelmi, R. Kneip, E. Flemming, H. Schmoranzer, M. Glass-Maujean, Collisional quenching of H(3 l) atoms by molecular hydrogen, J. Phys. B: At. Mol. Opt. Phys. 31 (1998) 3049 – 56. https://doi.org/10.1088/0953-4075/31/13/021

[38] K.W. Hemawan, T.A. Grotjohn, D.K. Reinhard, J. Asmussen, Improved microwave plasma cavity reactor for diamond synthesis at high-pressure and high power density, J. Diam. Relat. Mater. 19 (2010) 1446 – 52. https://doi.org/10.1016/j.diamond.2010.07.005

[39] N. Derkaoui, C. Rond, K. Hassouni, A. Gicquel, Spectroscopic analysis of H2/CH4 microwave plasma and fast growth rate of diamond single crystal, J. Appl. Phys. 115 (2014) 233301 1 – 8. https://doi.org/10.1063/1.4883955

[40] S. Barrat, S. Saada, I. Dieguez, E. Bauer-Gross, Diamond deposition by chemical vapor deposition process: Study of the bias enhanced nucleation step, J. Appl. Phys. 84 (1998) 1870 – 80. https://aip.scitation.org/doi/pdf/10.1063/1.368314

[41] Garg, R. K., Anderson, T. N., Lucht, R. P., Fisher, T. S., & Gore, J. P. (2008). Gas temperature measurements in a microwave plasma by optical emission spectroscopy under single-wall carbon nanotube growth conditions. Journal of Physics D: Applied Physics, 41(9), 095206. https://doi.org/10.1088/0022-3727/41/9/095206

APPENDIX

DC BIAS SET UP

1. The power supply for the DC bias needs to be connected to a power source. Then it has a ground (black) and a negative output (red).

2. The ground output needs to be connected to the chamber of the CVD

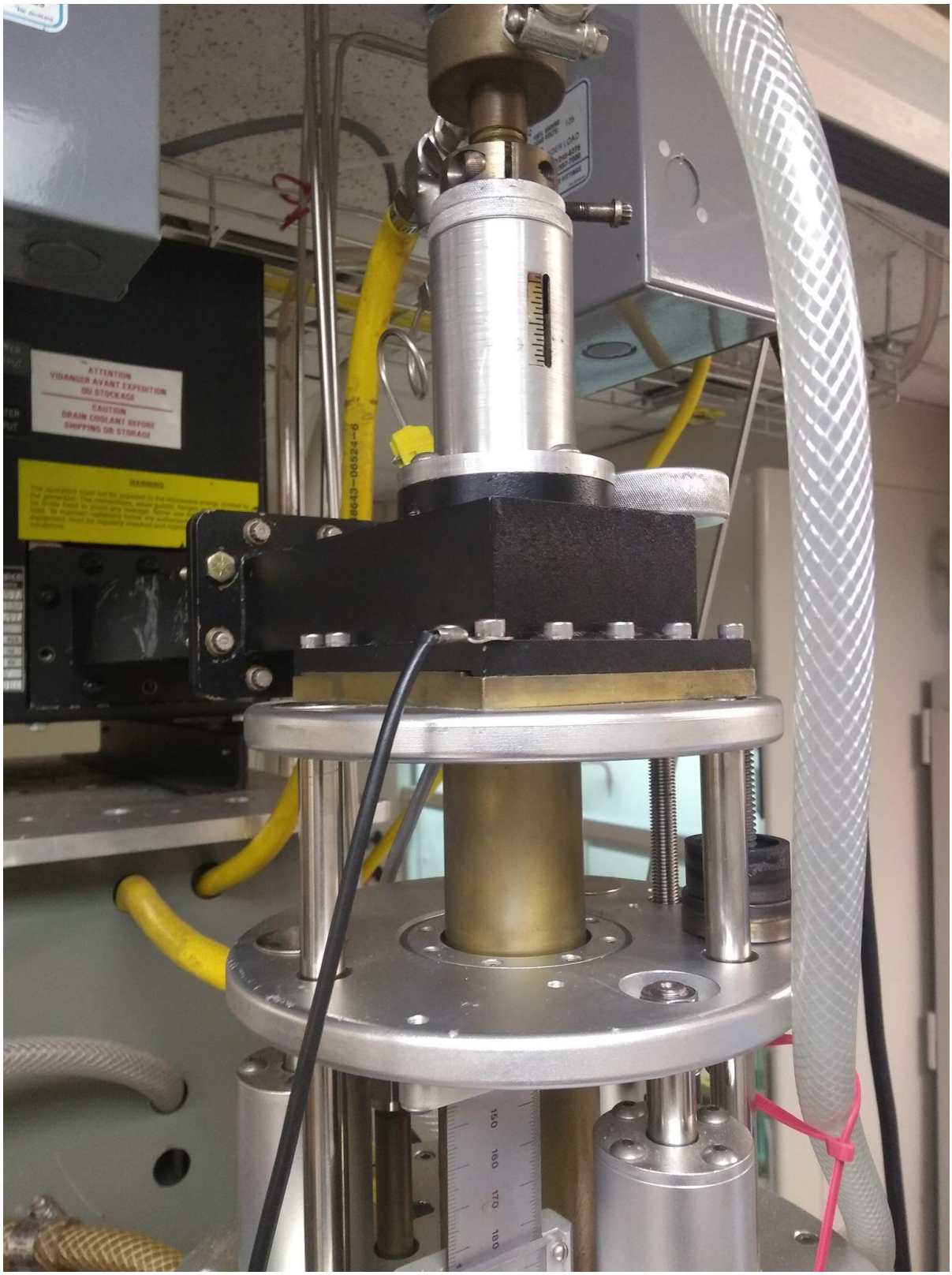
ATTENTION
VISANGER AVANT EXPEDITION
OU STOCKAGE
CAUTION
DRAIN COOLANT BEFORE
SHIPPING OR STORAGE
WARNING
8643-06524-6
150
160
170
180

3. The negative terminal need to reach the substrate through a port at the bottom of the CVD. The port itself is electrically insulated from the camber of the CVD. This is the outside connection of the port.

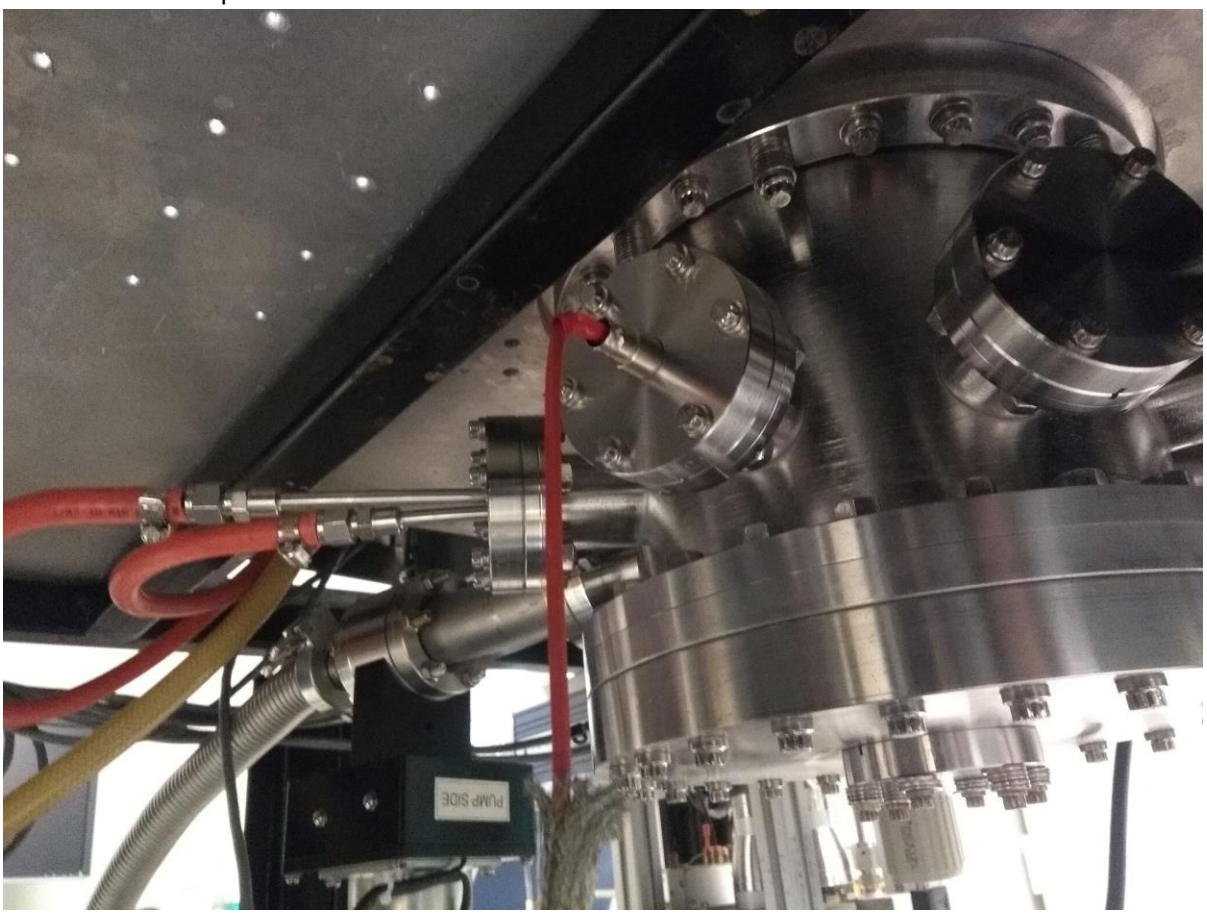

4. Inside, a cable will connect from the port to a substrate. The tape is electrically insulating, and high temperature rated ($\approx 200\,°C$). This prevents the electric wires from creating a short with the CVD body while the tape does not burn.

5. The screw onto which the substrate stands has a hole for the wire to connect.

6. Electrically isolate the screw from the molly plate by using the high temperature tape on the screw holder.

7. The crew holder should fit into the molly stage since the tape is thin. Use only one layer of the tape around the screw.

8. Test that the srew and substrate are electrically insulated from the molly stage holder. This allows ions to bombard the substrate and substrate holder only.

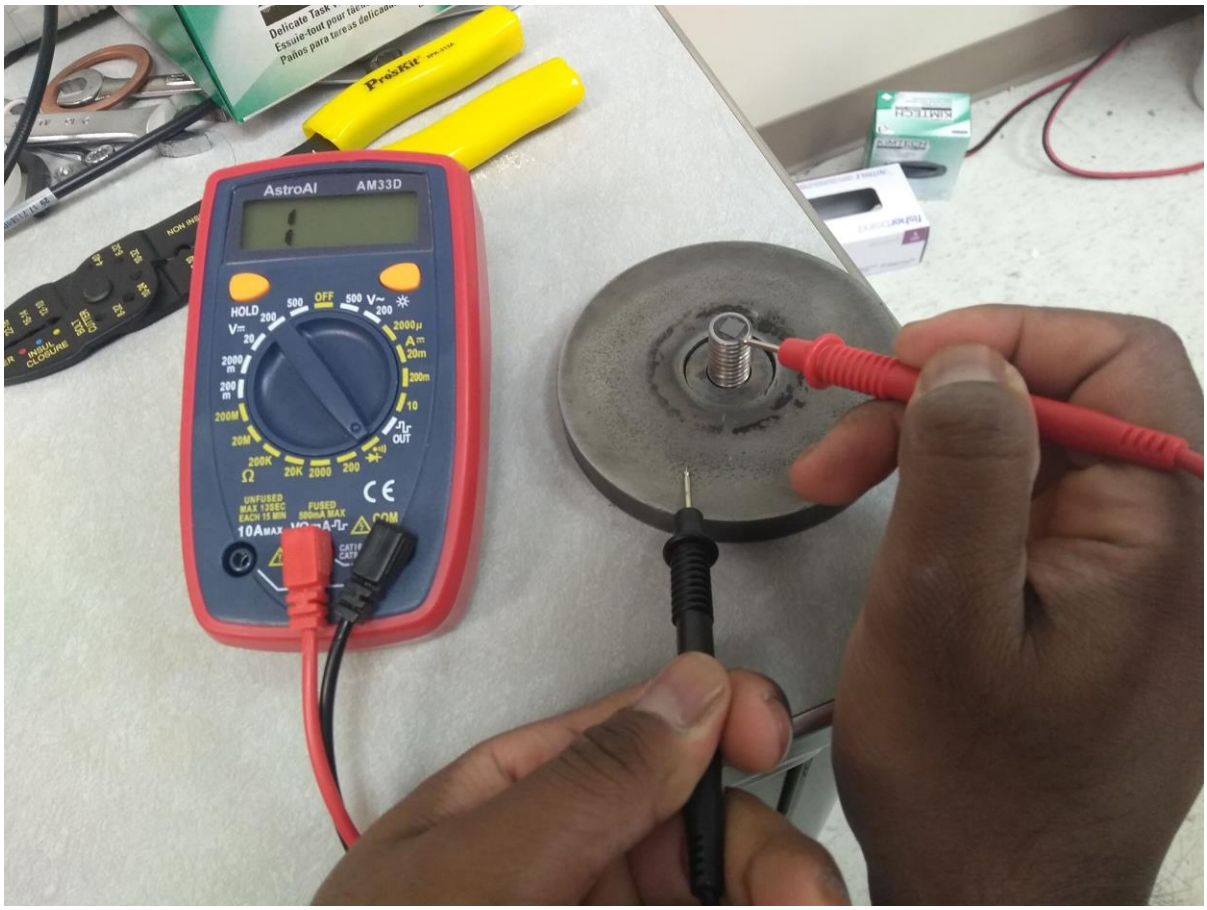

9. Avoid using gloves when working with the tape and testing for electrical conducted. Clean properly before leading the stage and substrate into the CVD. Use gloves.

10. Load the stage in the CVD.

11. Turn on bias voltage for testing. Turn to low voltage (<15 V) for lab safety. Current reading should be zero because there is not a complete connection between negatively biased screw and grounded CVD chamber. **(DO NOT COMPLETE THAT CONNECTION BY SIMULTANEOUSLY TOUCHING BOTH).** Let the ions from the plasma do that.

12. Test that the voltage between the screw and the CVD chamber is – 15V.

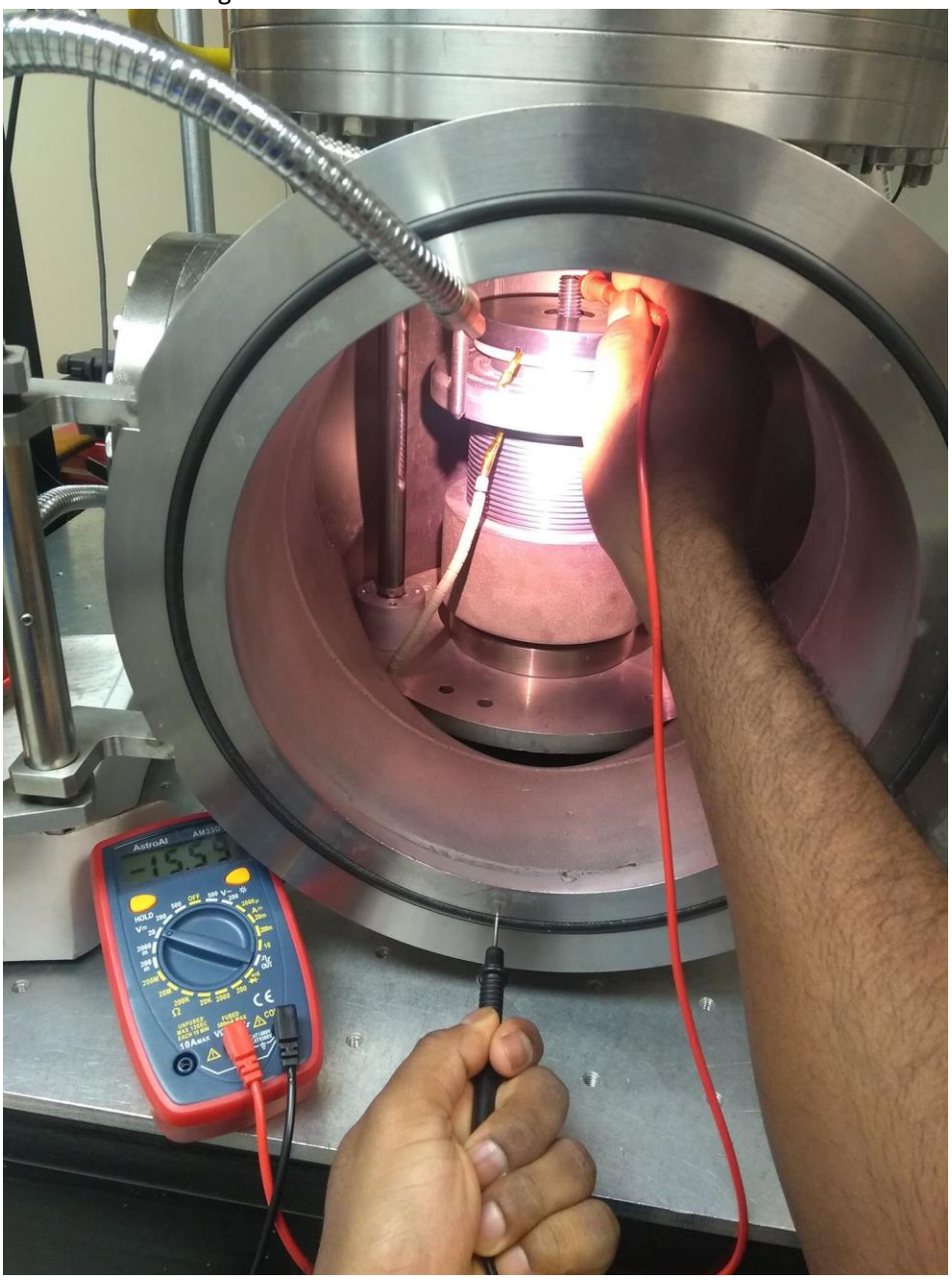

16. Since the screw is electrically insulated from the molly stage, check that the voltage between stage and the chamber is 0 V. If voltage is < 0V, check insulation again.

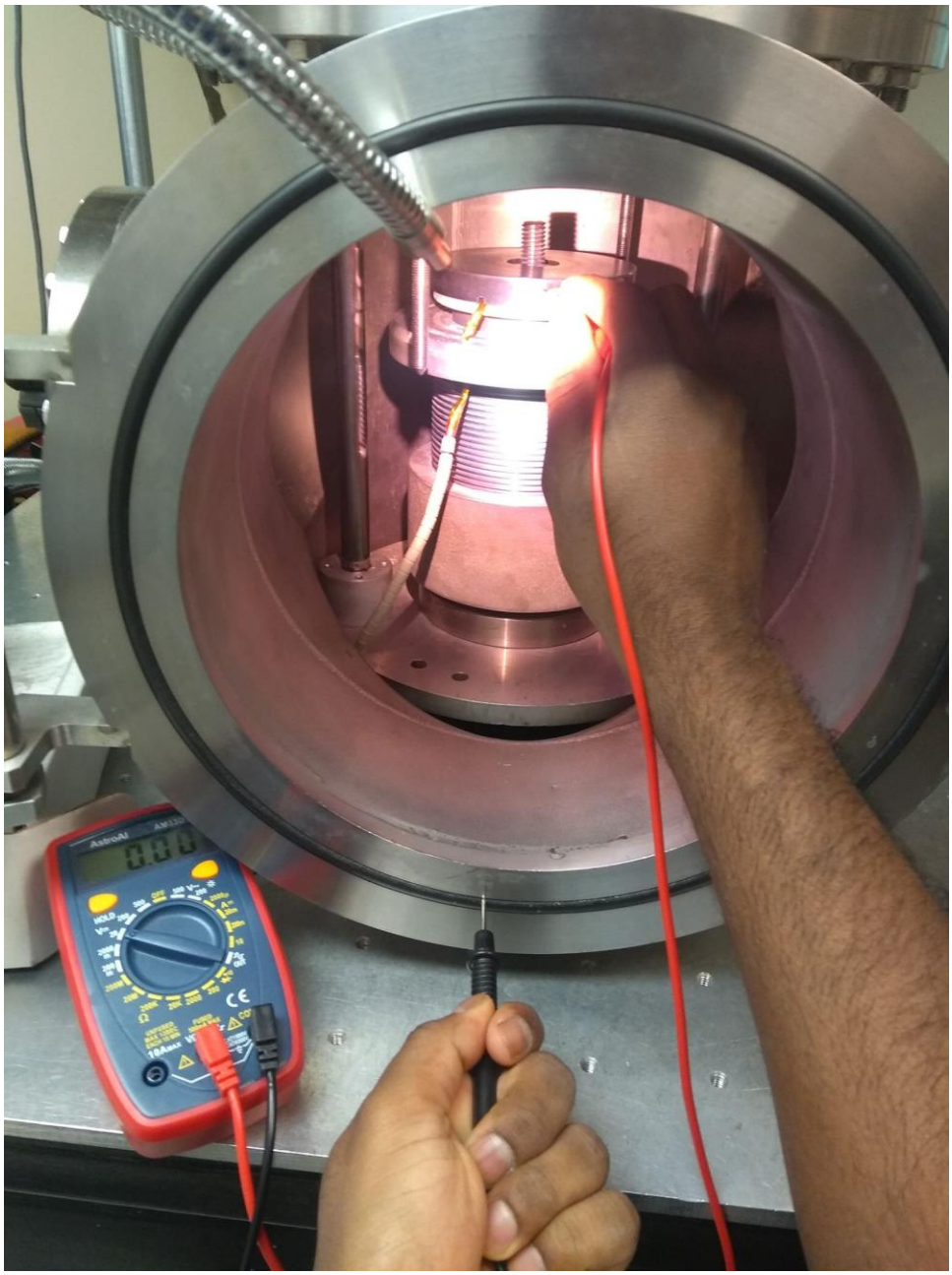

17. Follow lab procedures to clean CVD, substrate, substrate holders before running experiment.

18. The power supply will switch from voltage mode to current mode when there is a short between ions and the cable, or CVD chamber and the cable. Hence, electrical insulation needs to be regularly maintained (weekly). The insulation wears out after about 5 full experiments.